Networks of intergenic long-range enhancers and snpRNAs drive castration-resistant phenotype of prostate cancer and contribute to pathogenesis of multiple common human disorders

Anna B. Glinskii, Shuang Ma, Jun Ma, Denise Grant, Chang-Uk Lim, Ian Guest, Stewart Sell, Ralph Buttyan, Gennadi V. Glinsky

Translational and Functional Genomics Laboratory, Department of Pathology and Laboratory Medicine, and Department of Surgery, Division of Urology, Albany Medical College, Ordway Cancer Center, Ordway Research Institute, Inc., Center for Medical Science 150 New Scotland Ave, Albany, NY 12208; Genlighttechnologies Corporation, Inc., 939 Coast Blvd, Suite 4M, La Jolla, CA 92037

Email: genlighttec@gmail.com

Running title: intergenic trans-regulatory prostate cancer susceptibility snpRNAs

Key words: single nucleotide polymorphism; human SNP variations; prostate cancer susceptibility; non-coding RNAs; microRNAs; *NLRP1* (*NALP1*); translational genomics; microarray; gene expression; inflammasomes; innate immunity; apoptosis;

Abstract

Biological and mechanistic relevance of intergenic disease-associated genetic loci (IDAGL) containing highly statistically significant disease-linked SNPs remains unknown. Here we present the experimental and clinical evidence revealing important role of IDAGL in human diseases. Targeted RT-PCR screen coupled with sequencing of purified PCR products detects widespread transcription at multiple intergenic disease-associated genomic loci (IDAGL) and identifies 96 small non-coding trans-regulatory RNAs of ~ 100-300 nt in length containing SNPs associated with 21 common human disorders (snpRNAs). Functionality of snpRNAs is supported by multiple independent lines of experimental evidence demonstrating their cell-type-specific expression and evolutionary conservation of sequences, genomic coordinates, and biological effects. Analysis of chromatin state signatures, expression profiling experiments using microarray and Q-PCR technologies, and luciferase reporter assays indicate that many IDAGL are Polycomb-regulated long-range enhancers. Expression of snpRNAs in human and mouse cells markedly affects cellular behavior and induces allele-specific clinically-relevant phenotypic changes: *NLRP1*-locus SnpRNAs exert regulatory effects on monocyte/macrophage trans-differentiation, induce prostate cancer (PC) susceptibility SnpRNAs, and transform low-malignancy hormone-dependent human PC cells into highly malignant androgen-independent PC. Q-PCR analysis and luciferase reporter assays demonstrate that snpRNA sequences represent allele-specific “decoy” targets of microRNAs which function as SNP-allele-specific modifiers of microRNA expression and activity. We demonstrate that trans-acting RNA molecules facilitating androgen depletion-independent growth (ADIG) in vitro and castration-resistant (CR) phenotype in vivo of PC contain intergenic 8q24-locus SNP variants which were recently linked with increased risk of developing PC. Expression level of 8q24-locus PC susceptibility snpRNAs is regulated by *NLRP1*-locus snpRNAs, which are transcribed from the intergenic long-range enhancer

sequence located in 17p13 region at ~ 30 kb distance from the *NLRP1* gene. Q-PCR analysis of clinical PC samples reveals markedly increased snpRNA expression levels in tumor tissues compared to the adjacent normal prostate [122-fold and 45-fold in Gleason 7 tumors ($p = 0.03$); 370-fold and 127-fold in Gleason 8 tumors ($p = 0.0001$); for *NLRP1*-locus and 8q24-locus SnpRNAs, respectively]. Highly concordant expression profiles of the *NLRP1*-locus snpRNAs and 8q24 CR-locus snpRNAs ($r = 0.896$; $p < 0.0001$) in clinical PC samples and experimental evidence of trans-regulatory effects of *NLRP1*-locus snpRNAs on expression of 8q24-locus SnpRNAs indicate that ADIG and CR phenotype of human PC cells can be triggered by RNA molecules transcribed from the *NLRP1*-locus intergenic enhancer and down-stream activation of the 8q24-locus snpRNAs. Our results define the intergenic *NLRP1* and 8q24 regions as regulatory loci of ADIG and CR phenotype of human PC, reveal previously unknown molecular links between the innate immunity/inflammasome system and development of hormone-independent PC, and identify novel diagnostic and therapeutic targets exploration of which should be highly beneficial for clinical management of PC.

Introduction

Meta-analysis of genomic coordinates of nearly 800 significant SNP-phenotype associations ($P<5x10^{-8}$) identified in nearly 600 genome-wide association studies (GWAS) of 150 distinct diseases and traits demonstrates that only 12% of identified to date disease-linked SNPs are located within exons of protein-coding genes (or occur in tight linkage disequilibrium with protein-coding regions of genes) and a vast majority (80%) of variations occurs within non-protein-coding sequences (1). These findings are particularly striking because SNPs in protein-coding regions are heavily over-represented on genotyping arrays (2, 3) which further highlight the significant knowledge gap in our understanding the role of intronic and intergenic sequences in regulation of phenotypes. Intergenic SNPs, which are located in genomic regions distant from known protein-coding genes and microRNAs, comprise 40% and represent the largest class of SNP variations with significant associations to multiple common human disorders (4). Recently we reported identification of thirteen intergenic small trans-regulatory RNAs (trans-RNAs) containing disease-linked SNPs and manifesting cell type-specific patterns of expression in human cells (4). Functional analysis of one of these trans-RNAs, which are transcribed from the intergenic sequence located in 17p13 region at ~30 kb distance from the *NLRP1* gene and termed *NLRP1*-locus snpRNA, demonstrates SNP allele-specific biological effects of trans-RNAs on cell cycle progression, differentiation, and gene expression in human cells (4). These initial observations indicate that intergenic disease-associated genetic loci (IDAGL) are transcriptionally active and may influence the biological behavior of human cells via non-coding RNA intermediaries.

Several independent GWAS identified prostate cancer susceptibility SNPs within the 8q24 gene desert (5–12), which were subsequently classified into three adjacent genomic regions of

increased risk for prostate cancer (13). These regions contain multiple prostate cancer risk SNPs with the most significant and convincingly replicated SNPs being rs1447295 in region 1, rs16901979 in region 2, and rs6983267 in region 3 (13). Consistent with the hypothesis of biological significance of IDAGL, several groups reported that multiple long-range enhancers are present within genetically-defined prostate cancer risk regions of the 8q24 gene desert (14-18) and demonstrated functional correlations of enhancer's activity with prostate cancer risk SNP sequences.

In this work we report sequences of 96 snpRNAs which are transcribed from IDAGL that were discovered in association studies of common human disorders and replicated in independent cohorts of patients (Supplemental references 1-43). Functional analyses of snpRNAs associated with prostate cancer reveal novel genome-wide trans-regulatory networks of non-coding snpRNAs which are transcribed from long-range enhancers and facilitate development of castration-resistant phenotype of human prostate cancer. Our experiments indicate that activation of the *NLRP1*-locus snpRNA/miR-205 axis may contribute to development of clinically-significant prostate cancer by reducing expression of the *PTEN* tumor suppressor.

Results

IDAGL generate evolutionary conserved small non-coding snpRNAs and display common chromatin state signatures.

To date, we analyzed 109 IDAGL using targeted RT-PCR-based screening protocol which is designed for identification of RNA molecules containing disease-associated SNP sequences (4). We identified 96 trans-regulatory RNAs (snpRNAs) 100 to 300 nucleotides in length containing intergenic SNPs which are associated with 21 common human disorders (Supplemental Tables S1-S9). Molecular identities of discovered RNA molecules were established based on a requirement of reverse-transcription for detection of expected size PCR products and confirmed by size correspondence, sensitivity to RNAse treatment and resistance to DNAse treatment of primary PCR

products and nested PCR products which were derived from second round of amplification of purified primary PCR products. In all instances molecular identities of discovered RNA molecules were validated by direct sequencing of purified primary PCR products (Supplemental Tables S6-S9).

Considering the evidence of evolutionary conservation as one of the important criteria supporting the hypothesis of functionality of discovered snpRNA molecules, we analyzed a set of 13 IDAGL, which generate evolutionary conserved snpRNAs. Notably, 9 of 13 (70%) of evolutionary conserved intergenic sequences manifest common genomic topologies in the mouse and human genomes that is snpRNA-encoding sequences in both species have the same flanking protein-coding genes (Supplemental Figure S1). We made use of the extensive genome-wide chromatin domain maps (19, 20) to assess the chromatin state of evolutionary conserved IDAGL. This analysis reveals a consensus chromatin signature of evolutionary conserved snpRNA-encoding IDAGL comprising H3K27Me3, CBP/CREB, and POL2 proteins (Supplemental Figure S2), which indicate that IDAGL may represent a distinct class of Polycomb-regulated enhancers. Consistent with this notion, many evolutionary conserved snpRNA-encoding IDAGL display enhancer's signature H3K4me1 histone marks (Supplemental Figure 2), whereas histones H3K4Me3 and H3K36Me3, which represent chromatin signatures of promoters and transcriptionally active sites (21-23), appear less frequently. We confirmed the validity of these findings for both evolutionary-conserved and non-conserved IDAGL by performing the analysis of the chromatin state maps of IDAGL in human embryonic stem cells, ESC (Supplemental Figures 1-3; Supplemental Table S10). Based on this analysis we concluded that nearly ubiquitous chromatin state signature of IDAGL in human ESC consists of histone H3K27me3 and Ezh2 protein (Supplemental Figures 2 and 3). In addition to consensus components, the IDAGL chromatin maps display clearly discernable disorder-type-specific protein marks which manifest common association patterns for pathogenetically- and epidemiologically-related disease phenotypes (Supplemental Figure S4; Supplemental Table S10). Analysis of ENCODE chromatin state maps in 9 human cell lines validates this conclusions and reveals a

consensus chromatin signature of IDAGL comprising H3K27Me3 and H3K4Me1 histones, Ezh2, and disease-state-specific panels of transcription factors (http://genome.ucsc.edu/ENCODE/).

Expression of *NLRP1*-locus snpRNAs induces clinically-relevant phenotypic changes in human cells.

Given that SNP-phenotype associations can result from tagging and may therefore not necessarily indicate the true causal relationships, we thought to undertake the functional analysis of selected snpRNAs to show that snpRNA-mediated phenotype altering effects on cellular behavior reflect their role in diseases. Functional analysis of human cell lines engineered to constitutively express distinct allelic variants of *NLRP1*-locus snpRNAs revealed marked changes of biological behavior of cells expressing disease-associated allelic variants of snpRNAs which are consistent with targeted alterations of cell cycle progression/differentiation pathways (4). To ascertain whether changes of cellular functions caused by forced expression of *NLRP1*-locus snpRNAs are consistent with their suspected role in diseases, we analyzed monocyte/macrophage trans-differentiation of human THP-1 cells constitutively expressing 52 nt *NLRP1*-locus snpRNAs containing either ancestral, major A allele or disease-linked, minor G allele (Figure 1). We found that G-allele expressing THP-1 cells, in contrast to control or A-allele expressing cells, undergo massive apoptosis during differentiation process and are capable to generate 5-fold less macrophages compared to A-allele expressing cells (Figure 1A). Expression of snpRNAs containing ancestral A-allele confers protection against apoptosis and facilitates production of nearly two-fold more macrophages compared to control cells (Figure 1A). Notably, macrophages derived from A-allele-expressing THP-1 cells manifest significantly more potent phagocytic activity compared to control cells or macrophages derived from G-allele-expressing THP-1 cells (Figure 1A, inset). These phenotypic changes are not due to the generally diminished cellular functions because G-allele expressing cells manifest a

sustained long-term viability in optimal growth conditions and have significantly higher motility compared to the control cultures and A-allele expressing cells (Figure 1B).

Next we thought to determine whether the evolutionary conservation of *NLRP1*-locus snpRNAs is sufficient to facilitate the similar biological effects on mouse cells. We found that human *NLRP1*-locus snpRNAs exert biological effects on mouse macrophages and mesenchymal cells which are strikingly similar to that documented for human cells (Figure 1C, top panels). Furthermore, the allele-specific biological effects of forced expression *NLRP1*-locus snpRNAs mediated by the lentiviral gene transfer can be readily reproduced by transfection of synthetic LNA oligonucleotide analogues of snpRNA molecules (Figure 1C, bottom panels). Based on these observations we conclude that substitution of a single nucleotide in snpRNA molecules may cause dramatic alterations of cell's fate and results in marked changes of cellular phenotypes of potential clinical relevance.

NLRP1-locus snpRNAs transform low-malignancy hormone-dependent human PC cells into highly malignant castration-resistant PC by inducing 8q24-locus PCS-snpRNAs.

Q-RT-PCR expression profiling experiments reveal that *NLRP1*-locus snpRNAs markedly alter the expression of prostate cancer susceptibility (PCS) snpRNAs in human cells (Figure 2), which suggest that extensive phenotypically-relevant regulatory cross-talk may exist between distinct classes of snpRNAs. We noted particularly interesting patterns of association between expression of *NLRP1*-locus snpRNAs and 8q24-locus PCS-snpRNAs A6, expression of which appears elevated in highly metastatic variants of human prostate cancer cell lines as well as prostate cancer cell lines selected for growth in androgen-free media (Figure 2). To confirm that observations of clinically-relevant biological effects of IDAGL snpRNAs are not limited to the *NLRP1*-locus snpRNAs, we analyzed the effect of forced expression of distinct allelic variants of PCS-snpRNAs on behavior of hormone-dependent human prostate carcinoma cell line LNCap cultured under various growth conditions. We found that expression of both *NLRP1*-locus and PCS-snpRNAs have no effect on

growth of LNCap cells in adherent cultures (data not shown), whereas the anchorage-independent growth potential of LNCap cells in agar was markedly enhanced by PCS-snpRNAs A6, which was more significant for PCS-snpRNAs containing the prostate cancer susceptibility allele (Figure 2C). Human prostate carcinoma LNCap cells are hormone-dependent and are not capable of growing in androgen-free media (Figure 2C). Intriguingly, when we cultured in androgen-free conditions LNCap cells engineered to stably express snpRNAs, we found that expression of either *NLRP1*-locus snpRNAs or PCS-snpRNAs A6 facilitates hormone depletion-independent growth of LNCap cells (Figure 2C).

Highly metastatic LNCapLN3 cells which were selected for increased metastatic potential by serial orthotopic re-implantation after recovery from metastatic lesions acquire markedly increased ability to grow in agar and in androgen-depleted media (Figure 2C, insets). Q-RT-PCR expression profiling analysis reveals that LNCapLN3 cells manifest markedly higher expression level of the PCS-snpRNA A6 (Figure 2A). To determine whether altered grow properties of the highly metastatic LNCaLN3 cells are associated with increased expression of PCS-snpRNA A6, we engineered LNCapLN3 cell variants stably expressing anti-sense variants of the PCS-snpRNA A6 (AS-PCS-snpRNA A6). We found that expression of AS-PCS-snpRNA A6 did not affect growth of adherent cultures of LNCapLN3 cells in complete media (data not shown). In contrast, expression of AS-PCS-snpRNA A6 markedly diminishes growth of LNCapLN3 cells in agar cultures and in androgen-depleted media (Figure 2C, insets).

Parental LNCap cells are poorly tumorigenic in vivo and are not capable of forming tumors in castrated mice. Remarkably, when we inoculated LNCap cells engineered to stably express PCS-snpRNAs A6 (LNCap-A6 cells), all castrated mice developed rapidly growing, large tumors (Figure 2D), which appear to grow faster in castrated animals compared to sham-operated controls. As expected, no tumors were detected in castrated mice after inoculation of parental or control-transfected LNCap cells. These experiments demonstrate that stable expression of PCS-snpRNA A6

in low-malignancy, hormone-dependent human prostate carcinoma cells confers castration-resistant phenotype and facilitates androgen depletion-independent growth. Collectively, our clinical and experimental findings presented in Figures 2 and 3 indicate that prostate cancer cells which will emerge in individuals expressing high level of the prostate cancer susceptibility snpRNAs are more likely to acquire the intrinsic ability to grow in androgen-low or androgen-free conditions and, therefore, this type of prostate cancer is more likely to progress early to hormone-independent, incurable, metastatic disease.

Q-PCR analysis reveals markedly increased levels of *NLRP1*-locus snpRNAs and 8q24-locus PCS-snpRNAs in tumor tissue samples from prostate cancer patients diagnosed with clinically-significant early-stage disease.

To facilitate evaluation of the clinical significance of discovered RNA molecules, we developed and validated Q-PCR-based method of quantitative analysis of snpRNA expression. Our Q-PCR method of snpRNA expression demonstrates excellent reproducibility for both *NLRP1*-locus snpRNAs (r^2 = 0.808 for technical replicates) and 8q24-locus snpRNAs (r^2 = 0.888 for technical replicates) and > 8,000-fold dynamic range of detection's sensitivity in 3-5 ng of cDNA (Figure 3C). snpRNAs expression analysis in clinical PC samples reveals markedly increased snpRNA expression levels in tumor tissues compared to the adjacent normal prostate (Figure 3A and 3B). Notably higher expression levels of snpRNAs in human prostate adenocarcinoma samples and apparent association of increased snpRNA expression with pathohistological features of clinically-significant disease [122-fold and 45-fold in stage 2, Gleason 7 tumors (p = 0.03); 370-fold and 127-fold in stage 2, Gleason 8 tumors (p = 0.0001); for *NLRP1*-locus and 8q24-locus snpRNAs, respectively; Figure 3C] underscore potential translational relevance of our findings. Unexpectedly, we found a remarkably high correlation (r = 0.896; p < 0.0001) of expression levels of the *NLRP1*-locus snpRNAs and 8q24 ADIG-locus snpRNAs (r^2 = 0.803) in clinical PC samples (Figure 3C). We conclude that Q-PCR analysis of

clinical samples reveals pathophisiological relevance of discovered snpRNA molecules by demonstrating: 1) markedly increased expression levels in prostate cancer; 2) association of increased expression levels with pathohistological features of the clinically aggressive disease; 3) highly concordant expression profiles of snpRNAs transcribed from genetic loci located at distinct chromosomes (17p13 and 8q24). Collectively, these data indicate the presence of a novel trans-regulatory pathway which involves increased expression of intergenic snpRNAs transcribed from 17p13 and 8q24 loci and suggest co-selection of these regulatory features in clinically-significant prostate cancer.

snpRNAs are products of transcriptional activity of long-range intergenic enhancers.

Several intergenic PC risk SNPs were mapped to functional enhancer elements in human cells (14-18) suggesting that snpRNAs are products of transcriptional activity of long-range enhancers. Consistent with this idea, widespread transcription of neuronal activity-regulated enhancers in mice has been documented recently (19). We thought to investigate whether the *NLRP1*-locus IDAGL may assert the detectable allele-specific functional effect on transcription by cloning distinct allelic variants of the chemically-synthesized 2 kb *NLRP1* IDAGL region into the vector containing the firefly luciferase reporter, transfecting the purified experimental and control plasmids into target cells, and measuring the levels of luciferase activity. To control for transfection efficiency, the IDAGL-containing firefly luciferase reporter plasmids were co-transfected with plasmids containing a renilla luciferase reporter. We found that the presence of distinct allelic variants of IDAGL sequences significantly alter the expression of firefly luciferase (Figure 4), which suggest that IDAGL may function as SNP allele-specific intergenic enhancers/insulators and affect the transcription of protein-coding genes. DNA/RNA complementarily rules suggest that snpRNAs may affect the activity of corresponding enhancer elements. Consistent with this idea, both enhancer and insulator activities of the *NLRP1*-locus IDAGL are regulated by *NLRP1*-locus snpRNAs (Figure 4). The enhancer/insulator functions of

IDAGL/snpRNA feed-back regulatory loops appear specific because they are dependent on the SNP allele status of both DNA and RNA sequences (Figure 4 and data not shown).

NLRP1-locus snpRNAs regulate expression of 14q32 locus microRNAs.

Analysis of the predicted secondary structures of identified RNA molecules reveals that one of the notable common features of snpRNAs secondary structures is the presence of loop sequences which contain SNP-bearing 8-11 nt segments identical to primary sequences of microRNAs (Supplemental Figure S5). Intergenic snpRNA sequences contain multiple potential target sites for microRNAs which are often clustered around SNP nucleotides (Supplemental Figure S5). These data suggest that an epigenetic regulatory cross-talk between snpRNAs and microRNAs may exist with the potential down-stream effect on expression of protein-coding genes. Analysis of human cell lines engineered to stably express distinct allelic variants of the *NLRP1*-locus snpRNAs confirmed the validity of this hypothesis (4). Expression profiling experiments identify 36 microRNAs differentially regulated in BJ1 cells expressing distinct allelic variants of the *NLRP1*-locus snpRNAs (Figure 5 and Supplemental Figure S6). Analysis of genomic coordinates reveals that genes encoding 18 of 36 (50%) *NLRP1*-locus snpRNA-regulated microRNAs are located within ~ 200 kb regions on 14q32 which is immediately adjacent to the long non-coding RNA gene, *MEG3* (Supplemental Figures S6-S7). Thus, our analysis demonstrates that principal molecular targets for allele-specific trans-regulatory actions of *NLRP1*-locus snpRNAs are clusters of microRNAs within a 200 kb segment of the 14q32 region which is adjacent to the snpRNA-targeted long non-coding RNA gene, *MEG3*. Detailed exploration of individual snpRNA-regulated transcripts shows that expression levels of distinct classes of non-coding RNAs are significantly altered in human cells engineered to stably express *NLRP1*-locus snpRNAs (Supplemental Figure S6). These results indicate that one of the important epigenetic features of snpRNA-mediated regulatory effects is genome-wide changes in expression of multiple diverse classes of non-coding RNAs documented examples of which include

snoRNAs and snoRNA-host genes (*SNORD113; SNHG1; SNHG3; SNHG8*); long non-coding RNAs (*MEG3, HOTAIR, tncRNA,* and *MALAT1*); microRNAs, microRNA-precursors, and protein-coding genes introns of which host microRNA genes (*ATAD2; KIAA1199;* Supplemental Figure S6).

Allele affinity model of snpRNA-mediated regulation of microRNA expression and activity.

To understand the molecular basis of the regulatory cross-talk between snpRNAs and a diverse network of non-coding RNAs, we performed sequence homology profiling and structure-functional analysis of relevant molecular entities. This analysis shows that snpRNA-regulated non-coding RNAs manifest discernable homology/complementarity features of primary sequences. Notably, all 36 *NLRP1*-locus snpRNA-regulated microRNAs have at least one potential target sites within 152 nt sequence of the *NLRP1*-locus snpRNA molecule and many microRNA target sites manifest allele-associated changes of the minimal free energy (mfe) snpRNA/microRNA hybridization (Figure 5, Supplemental Figures S5 – S7). Comparisons of the allele-associated changes of the mfe values and experimentally-defined changes of the microRNA expression levels reveal a highly significant inverse correlation between these two variables that is lower mfe values appear to correspond to higher levels of microRNA expression (Figure 5 and Supplemental Figure S8). These results suggest a model of snpRNA-mediated regulation of microRNA expression according to which high affinity (low mfe) snpRNA alleles would facilitate increase abundance levels of corresponding microRNAs (Figure 5 and Supplemental Figure S8).

Recent experiments demonstrate that let-7 microRNA release from complexes with Argonaute proteins and subsequent degradation can both be blocked by addition of microRNA target RNA which results in increase let-7 microRNA level (24). Computer modeling experiments demonstrate that let-7b microRNA follows the pattern of allele-associated mfe changes characteristic of microRNAs expression levels of which are lower in G-allele expressing cells (Figure 5 and Supplemental Figure

S6D). We reasoned that if let-7 bioactivity model is valid for snpRNA-mediated effects on microRNAs, we should be able to detect the corresponding snpRNA allele-context-specific changes of the let-7b expression and activity in *NLRP1*-locus snpRNA-expressing cells. Consistent with this hypothesis, Q-PCR experiments and luciferase reporter assays demonstrate that both expression and activity of the let-7 microRNA are significantly modified in RWPE1 cells genetically engineered to stably express *NLRP1*-locus snpRNAs (Figure 5 and Supplemental Figure S8D). We confirmed the validity of these conclusions by documenting similar relationships between snpRNA allele-context-specific mfe changes and effects on microRNA expression and activity for miR-205 microRNA (Figure 5 and Supplemental Figure S8D, bottom panels). Based on these observations, we propose that one of the mechanisms of snpRNA-mediated effects on microRNA-regulated processes is associated with snpRNA-allele-specific changes of microRNA abundance level and activity. The underlying molecular events are likely to resemble the let-7 bioactivity model according to which interaction of RNA molecules with microRNAs interfer with microRNA release from complexes with Argonaute proteins and prevent subsequent degradation of microRNA (24).

***NLRP1*-locus snpRNA-regulated microRNAs recapitulate molecular features and biological phenotypes induced by snpRNAs.**

Microarray analysis demonstrates that epigenetic reprogramming of human cells following activation of the *NLRP1*-locus snpRNA-regulated network of non-coding RNAs involves thousand's down-steam protein-coding targets including 586 transcripts encoded by Polycomb-regulated bivalent chromatin domain genes (4) and 209 mRNAs encoded by human homologues of mouse genes flanking intergenic enhancers (data not shown). Collectively, these results as well as functional data support the model of sequential regulatory pathway of *NLRP1*-locus snpRNAs > microRNAs > protein-coding transcripts. Further analysis of the regulatory circuitries of this network reveals

markedly altered expression of prostate susceptibility snpRNAs in cell lines genetically engineered to stably express either *NLRP1*-locus snpRNAs or snpRNA-regulated microRNAs (Figure 5 and Supplemental Figure S8). Results of these experiments demonstrate that:

1) Constitutive expression of *NLRP1*-locus snpRNAs enhances expression levels of several microRNAs (Figure 6 and Supplemental Figures S8 and S9) and induces expression of prostate cancer susceptibility snpRNAs (Figure 2 and Supplemental Figure S8);

2) Expression of cancer susceptibility snpRNAs is similarly induced in cells engineered to over-express either *NLRP1*-locus snpRNAs or snpRNA-regulated microRNAs (Supplemental Figure S8);

3) Forced expression of selected snpRNA-regulated microRNAs recapitulate snpRNA-induced phenotypic changes in human cells such as the increased propensity for anchorage-independent growth in agar and enhanced clonogenic growth potential (Figure 6 and Supplemental Figure S8);

4) Microarray analysis of protein-coding transcripts in human cells engineered to over-express either *NLRP1*-locus snpRNAs or snpRNA-regulated microRNAs identifies common gene expression signatures (GES) expression profiles of which distinguishes highly metastatic human prostate carcinoma cell lines versus parental counterparts (Figure 6), clinical samples of distant metastatic lesions versus primary prostate tumors (Figure 6), and prostate cancer patients with significantly distinct likelihood of therapy failure after radical prostatectomy (Figure 6).

Interestingly, forced expression of miR-205 recapitulate many molecular, phenotypic, and clinical features associated with expression of *NLRP1*-locus snpRNAs (Figure 6), including markedly decreased expression of the *PTEN* tumor suppressor. These data in conjunction with the experimental evidence of *NLRP1*-locus snpRNA-induced expression and activity of miR-205 in human cells (Figure 5) indicate that activation of the *NLRP1*-locus snpRNA/miR-205 axis may contribute to development of clinically-significant prostate cancer.

Discussion

GWAS identify highly significant SNP-phenotype associations ($P<5x10^{-8}$) vast majority of which (80%) occurs within non-protein-coding sequences (1). These consistent and reproducible findings highlight a major knowledge gap in our understanding of phenotype-defining functions of human genome segments lacking protein-coding potentials. Our experiments reveal widespread transcription at IDAGL raising the possibility that non-protein-coding RNA molecules may play an important role in predisposition to multiple common human disorders. We demonstrate that forced expression of 52 nt snpRNAs imposes castration-resistant phenotype on human prostate carcinoma cells. It transforms low-malignancy, hormone-dependent human prostate cancer cells into highly malignant, androgen depletion-independent prostate cancer. To facilitate the assessment of clinical significance of discovered snpRNAs, we developed Q-PCR method of quantitative analysis of snpRNAs and validated its utility by analysis of snpRNA expression in clinical samples. Our analysis reveals markedly elevated snpRNA expression levels in prostate cancer tissues compared to the adjacent normal prostate (Figure 3). Notably higher expression levels of snpRNAs in human prostate adenocarcinoma samples and apparent association of increased snpRNA expression with pathohistological features of clinically-significant disease (high Gleason score) highlight potential translational relevance of our findings. Collectively, our data imply that prostate cancer cells which emerge in individuals expressing high levels of the prostate cancer susceptibility snpRNAs are more likely to progress early to hormone-independent, incurable, metastatic disease. Our work defines the intergenic 8q24 region as ADIG-regulatory locus of critical significance for human prostate cancer, reveals previously unknown molecular links between the innate immunity/inflammasome system and development of hormone-independent PC, and identify novel diagnostic and therapeutic targets successful validation of which should be highly beneficial for clinical management of prostate cancer patients.

Our experiments demonstrate that IDAGLs represent multifunctional genomic trans-regulatory domains possessing broad-range of intrinsic regulatory functions which are mediated by both DNA

sequences and transcribed RNA molecules. Many IDAGLs harbor a consensus chromatin signature comprising H3K27Me3 and H3K4Me1 histones, Ezh2, and disease-state-specific panels of transcription factors. IDAGL's functions as cell-type-specific long-range enhancers or insulators appear dependent on the allelic status of a disease-linked SNP and are regulated by snpRNAs. Our experiments indicate that microRNAs which have complementary sequences in corresponding snpRNAs may constitute one of the primary targets of snpRNA-induced genome-wide epigenetic regulatory networks engagement of which is triggered by distinctive single-base-level molecular recognition events (Supplemental Figure S8). Altered microRNA expression and activity would facilitate an epigenetic amplification of a single-base-driven regulatory event by inducing down-stream mRNA expression changes of many (perhaps, thousands) protein-coding genes which would ultimately cause clinically significant alterations of cellular functions. Examples of experimentally identified components of such a regulatory network are key inflammasome/innate immunity pathway-related genetic targets (4). In agreement with this mechanism, we found markedly altered expression of prostate cancer susceptibility snpRNAs in cell lines genetically engineered to stably express either *NALP1*-locus snpRNAs or snpRNA-regulated microRNAs (Figure 2 and Supplemental Figure S8). Further, our data suggest that microRNAs may contribute to biogenesis of snpRNAs by guiding Argonaute family-endonucleases to execute a sequence-specific cleavage of snpRNAs and putative small snpRNA-precursors, long non-coding snpRNAs. Consistently, we found that many small snpRNAs exhibit cell type specific expression profiles, whereas long non-coding snpRNAs containing disease-associated SNP sequences manifest more ubiquitous expression patterns (4). These observations indicate that small snpRNAs may represent products of a cell type-specific processing of long non-coding snpRNAs and support the hypothesis that microRNAs are intrinsic regulatory components of snpRNA/enhancer IDAGL networks which are contributing to maintenance of epigenetic regulatory state in a cell.

Our experiments indicate that activation of the *NLRP1*-locus snpRNA/miR-205 axis may contribute to development of clinically-significant prostate cancer by reducing expression of the *PTEN* tumor suppressor. We found that *NLRP1*-locus snpRNAs induce expression and activity of miR-205 in human cells (Figure 5) and forced expression of miR-205 recapitulate many molecular, phenotypic, and clinical features associated with expression of *NLRP1*-locus snpRNAs (Figure 6), including markedly decreased expression of the *PTEN* tumor suppressor. *PTEN* tumor suppressor has been identified as a target for miR-205 based on target prediction algorithms and miR-205 overexpression experiments using the pGL3-PTEN 3'UTR reporter constructs with mutations of miR-205-binding sites, microarray and TaqMan Q-PCR analyses, and western blot analysis (25). Altered expression and activity of miR-205 have been associated with epithelial-to-mesenchymal transition (EMT), emergence of stem cell-like properties, and maintenance of mammary epithelial cell progenitors (25-27).

Results of our experiments are highly consistent with the emerging concept of the pervasive, global transcriptional activity of human genomes which is supported by observations that vast majority of transcripts in human cells is represented by non-coding RNAs (28-37; see Supplemental text for discussion and additional references). Collectively, they lend credence to the idea that intergenic DNA sequence variations may contribute to disease pathogenesis via non-coding RNA intermediaries which assert trans-regulatory effects on epigenetic regulatory circuitry of a cell. This concept challenges the dominant position of protein-centric experimental paradigm that is focused on analysis of effects of genetic variations on protein-coding genes within or near boundaries of which the genetic variants are located. Conclusive evidence of ubiquitous expression in human cells of intergenic disease-associated genetic loci indicates the potential clinical benefits of the concurrent analyses of DNA sequences and expression profiling of corresponding RNA products. This is critically important because the transcriptional activity and transcript abundance levels are genetically-defined quantitative traits assessment of which should enhance the disease risk prediction power of

corresponding genetic tests. We anticipate that reported here findings should have a major near-term implication on design and execution of genome-wide association studies and follow-up mechanistic studies of non-protein-coding disease-linked loci. To this end, we provide sequences of validated primers and experimental protocols (Supplemental Tables S1-S5) to facilitate the immediate implementation of this type of analyses for 96 intergenic SNPs associated with increased risk of developing 21 common human disorders.

Methods

Detailed description of all aspects of the experimental procedures, including snpRNAs and microRNA isolation and activity analysis; microRNA expression analysis; Cell Staining and Flow Cytometry; Induced Differentiation of THP-1 cells; Lentivirus Production and Generation of Stably Transfected BJ1, RWPE1, U937, and THP-1 cells; Colony Growth and Clonogenic Growth Assays; can be found in the online Supplement and previous publications (4). Supplemental information is available at http://www.genlighttechnology.com

Cell Lines

Human BJ1, U937, THP-1, RWPE1, and HME1 cell lines were obtained from ATCC. hTERT-immortalized BJ1, LNCap, and LNCapLN3 cells were previously described (38-42).

Tumor Cell Xenografts. Sub-confluent monolayers of control LNCaP or LNCaP-A6 cells were trypsinized and counted, then resuspended in RPMI-1640 medium with 25% charcoal-dextran stripped-fetal bovine serum (CDS-FBS) and 50% (vol/vol) 2 X Matrigel (Millipore, Inc., Billerica, MA). Aliquots (250 µls) containing 10^6 cells were then injected subcutaneously in the flanks of 8-week male NCR Nu/Nu mice (Taconic, Inc.) that had been surgically castrated 10 days prior through a scrotal incision under anesthesia or sham-castrated involving the scrotal incision without removal of the testis. Tumor size was estimated from largest diameter (a), smallest diameter (b) and height (c) measurements with calipers with tumor volume calculated using the formula $V = \pi/6 \times a \times b \times c$. Mice

were euthanized at the end of the experiments, tumors were surgically recovered, weighted, and processed for pathological and molecular analyses.

Microarray gene expression analysis

Technical and analytical aspects as well as stringent QC and statistical protocols of gene expression analysis experiments was carried-out essentially as described in our published work (39-42). Briefly, the array hybridization and processing, data retrieval and analysis was carried out using standard sets of the Affymetrix equipment, software, and protocols in state-of-the-art Affymetrix microarray core facility. RNA was extracted from cell cultures of two independent biological replicates of each experimental condition and analyzed for sample purity and integrity using BioAnalyzer (Agilent). Expression analysis of 54,675 transcripts was carried out for each sample in duplicates using Affymetrix HG-U133A Plus 2.0 arrays. Data retrieval and analysis was performed using MAS5.0 software and concordant changes of gene expression for each experimental condition were determined at the statistical threshold p value < 0.05 (two-tailed T-test). All microarray analysis data are publicly available coincidently with the date of publication.

Protocols for identification of endogenous trans-regulatory RNAs

(Detailed descriptions of protocols A - E are presented in the Supplement)

1. Extract small RNA from cells using mirVana isolation kit (protocol A)
2. Detect if there is DNA contamination by performing PCR using extracted RNA as template and β-actin primers (protocol B)
3. Synthesize cDNA from extracted small RNA (protocol C)
4. Perform first-round PCR using appropriate primer set (protocol B)
5. Clean up PCR product and evaluate cleanup PCR product on 1.2% gel (protocol D)
6. Perform nested PCR using purified product of the first-round PCR as template and appropriate primer set; evaluate nested PCR product on 1.2% gel (protocol B)

7. Cut the single DNA band of interest from the gel, extract and purify the product for sequencing (protocol E)

Luciferase reporter assays

Luciferase reported assays were carried-out to identify allele-specific features of SNP-bearing RNA and DNA sequences. Enhancer/insulator activities of the 2 kb intergenic DNA sequence containing distinct allelic variants of the rs2670660 NLRP1-locus SNP. Luciferase reporter assays to assess the enhancer activity of 2 kb NALP1-locus intergenic region was carried out in RWPE1 and HEK293 cells transiently expressing either control luciferase reporter plasmids or plasmids containing chemically synthesized 2 kb sequences flanking distinct allelic variants of the *NLRP1*-locus intergenic SNP rs2670660, which is positioned exactly in the middle of the enhancer's sequence. Because allelic differences in the luciferase reporter assays tend to be modest, measurements were controlled by multiple replications of all experimental elements of the enhancer assay. We considered the possibility of multiple levels of variations, including plasmid preps, transfection replicates (along with transfection efficiency measurements, such as using the Renilla lucferase co-transfection controls for normalization). At least three independent experiments were carried out for each setting and three replicates of the luciferase assay were performed in each experiment. Results were validated using at least two independent plasmid preps to control for this potentially significant source of variation.

Statistical and Bioinformatics Analysis

Detailed protocols for data analysis and documentation of the sensitivity, reproducibility, and other aspects of the quantitative statistical microarray analysis using Affymetrix technology have been reported previously (39-42). Forty to sixty percent of the surveyed genes were called present by Affymetrix Microarray Suite version 5.0 software in these experiments. The concordance analysis of differential gene expression across the data sets was performed using Affymetrix MicroDB version 3.0 and DMT version 3.0 software as described previously (39-42). We processed the microarray data using the Affymetrix Microarray Suite version 5.0 software and performed statistical analysis of

the expression data set using the Affymetrix MicroDB and Affymetrix DMT software. The Pearson correlation coefficient for individual test samples and the appropriate reference standard were determined using GraphPad Prism version 4.00 software (GraphPad Software). We calculated the significance of the overlap between the lists of differentially-regulated genes by using the hypergeometric distribution test (43). Analyses of the predicted secondary structures of identified snpRNAs, screening for potential target sites of microRNAs, and sequence homology profiling of snpRNAs and microRNAs were performed using web-accessible publicly available resources (http://rna.tbi.univie.ac.at/cgi-bin/RNAfold.cgi; http://www.ncrna.org/centroidfold/; http://bioinfo.uni-plovdiv.bg/microinspector/; http://www.mirbase.org/).

Author Contributions

Conceived idea and conceptualized framework of the experimental work: GVG.

Conceived and designed the experiments: GVG ABG.

Performed the experiments: SM JM DG CL IG RB.

Analyzed the data: GVG ABG SM JM DG CL RB.

Contributed reagents/materials/analysis tools/financial support: GVG ABG SS RB.

Wrote the paper: GVG.

Acknowledgements

This work was supported, in part, by the grants from the National Institute of Health and Charitable Leadership Foundation (CLF), Clifton Park, NY.

References

1. Manolio, TA. Genomewide association studies and assessment of the risk of disease. N Engl J Med. 2010;363:166-176.

2. Hindorff LA, Sethupathy P, Junkins HA, et al. Potential etiologic and functional implications of genome-wide association loci for human diseases and traits. Proc Natl Acad Sci U S A. 2009;106:9362-7.

3. Hardy J, Singleton 1. A. Genomewide association studies and human disease. N Engl J Med. 2009;360:1759-68.

4. Glinskii, AB, Ma, J, Ma, S, Grant, D, Lim, C, Sell, S, Glinsky, GV. Identification of intergenic trans-regulatory RNAs containing a disease-linked SNP sequence and targeting cell cycle progression/differentiation pathways in multiple common human disorders. Cell Cycle 2009;8:3925-42.

5. Yeager M, et al. Genome-wide association study of prostate cancer identifies a second risk locus at 8q24. Nat Genet 2007;39:645–649.

6. Amundadottir LT, et al. A common variant associated with prostate cancer in European and African populations. Nat Genet 2006;38:652–658.

7. Gudmundsson J, et al. Genome-wide association study identifies a second prostate cancer susceptibility variant at 8q24. Nat Genet 2007;39:631–637.

8. Haiman CA, et al. Multiple regions within 8q24 independently affect risk for prostate cancer. Nat Genet 2007;39:638–644.

9. Freedman ML, et al. Admixture mapping identifies 8q24 as a prostate cancer risk locus in African-American men. Proc Natl Acad Sci USA 2006;103:14068–14073.

10. Tomlinson I, et al.; CORGI Consortium A genome-wide association scan of tag SNPs identifies a susceptibility variant for colorectal cancer at 8q24.21. Nat Genet 2007;39: 984–988.

11. Zanke BW, et al. Genome-wide association scan identifies a colorectal cancer susceptibility locus on chromosome 8q24. Nat Genet 2007;39:989–994.

12. Haiman CA, et al. (2007) A common genetic risk factor for colorectal and prostate cancer. Nat Genet 2007;39:954–956.

13. Witte JS Multiple prostate cancer risk variants on 8q24. Nat Genet 39:579–580.

14. Pomerantz MM., et al. The 8q24 cancer risk variant rs6983267 demonstrates long-range interaction with MYC in colorectal cancer. Nat Genet. 2009;41: 882–884.

15. Jia L, Landan G, Pomerantz M, Jaschek R, Herman P, et al. (2009). Functional Enhancers at the Gene-Poor 8q24 Cancer-Linked Locus. PLoS Genet 2009;5(8): e1000597.

16. Sotelo J., Esposito D, Duhagon MA., et al. Long-range enhancers on 8q24 regulate c-Myc. PNAS 2010;107:3001-3005.

17. Wright JB, Brown SJ, Cole MD. Upregulation of c-MYC in cis through a Large Chromatin Loop Linked to a Cancer Risk-Associated Single-Nucleotide Polymorphism in Colorectal Cancer Cells. Mol Cell Biol 2010;30: 1411–1420.

18. Wasserman NF, Ivy Aneas I, Nobrega MA. An 8q24 gene desert variant associated with prostate cancer risk confers differential in vivo activity to a MYC enhancer. Genome Res 2010;20: 1191-1197.

19. Kim TK, Hemberg M, Gray JM, Costa AM, Bear DM, Wu J, Harmin DA, Laptewicz M, Barbara-Haley K, Kuersten S, Markenscoff-Papadimitriou E, Kuhl D, Bito H, Worley PF, Kreiman G, Greenberg ME. Widespread transcription at neuronal activity-regulated enhancers. Nature. 2010;465:182-7.

20. Ku M, Koche RP, Rheinbay E, Mendenhall EM, Endoh M, Mikkelsen TS, Presser A, Nusbaum C, Xie X, Chi AS, Adli M, Kasif S, Ptaszek LM, Cowan CA, Lander ES, Koseki H, Bernstein BE. Genome wide analysis of PRC1 and PRC2 occupancy identifies two classes of bivalent domains. PLoS Genet. 2008;4: e1000242.

21. Heintzman, N. D. et al. Distinct and predictive chromatin signatures of transcriptional promoters and enhancers in the human genome. Nature Genet. 2007;39, 311–8.

22. Visel, A. et al. ChIP-seq accurately predicts tissue-specific activity of enhancers. Nature 2009;457, 854–858.

23. Xi, H. et al. Identification and characterization of cell type-specific and ubiquitous chromatin regulatory structures in the human genome. PLoS Genet. 2007;3, e136.

24. Chatterjee S, Grosshans H. Active turnover modulates mature microRNA activity in Caenorhabditis elegans. Nature. 2009;461:546-9.

25. Greene SB, Gunaratne PH, Hammond SM, Rosen JM. A putative role for microRNA-205 in mammary epithelial cell progenitors. J Cell Sci. 2010;123:606-18.

26. Ibarra I, Erlich Y, Muthuswamy SK, Sachidanandam R, Hannon GJ. A role for microRNAs in maintenance of mouse mammary epithelial progenitor cells. Genes Dev. 2007;21:3238-43.

27. Tellez CS, Juri DE, Do K, Bernauer AM, Thomas CL, Damiani LA, Tessema M, Leng S, Belinsky SA. EMT and Stem Cell-Like Properties Associated with miR-205 and miR-200 Epigenetic Silencing Are Early Manifestations during Carcinogen-Induced Transformation of Human Lung Epithelial Cells. Cancer Res. 2011;71(8):3087-97.

28. Bertone P, Stolc V, Royce TE, Rozowsky JS, Urban AE, Zhu X, Rinn JL, Tongprasit W, Samanta M, Weissman S, Gerstein M, Snyder M. Global identification of human transcribed sequences with genome tiling arrays. Science 2004; 306:2242-6.

29. ENCODE Project Consortium. Identification and analysis of functional elements in 1% of the human genome by the ENCODE pilot project. Nature 2007; 447:799-816.

30. Washietl S, Pedersen JS, Korbel JO, Stocsits C, Gruber AR, Hackermüller J, Hertel J, Lindemeyer M, Reiche K, Tanzer A, Ucla C, Wyss C, Antonarakis SE, Denoeud F, Lagarde J, Drenkow J, Kapranov P, Gingeras TR, Guigó R, Snyder M, Gerstein MB, Reymond A, Hofacker IL, Stadler PF. Structured RNAs in the ENCODE selected regions of the human genome. Genome Res 2007; 17: 852-64.

31. Rozowsky JS, Newburger D, Sayward F, Wu J, Jordan G, Korbel JO, Nagalakshmi U, Yang J, Zheng D, Guigó R, Gingeras TR, Weissman S, Miller P, Snyder M, Gerstein MB. The DART classification of unannotated transcription within the ENCODE regions: associating transcription with known and novel loci. Genome Res 2007; 17:732-45.

32. Kapranov P, Cheng J, Dike S, Nix DA, Duttagupta R, Willingham AT, Stadler PF, Hertel J, Hackermüller J, Hofacker IL, Bell I, Cheung E, Drenkow J, Dumais E, Patel S, Helt G, Ganesh M, Ghosh S, Piccolboni A, Sementchenko V, Tammana H, Gingeras TR. RNA maps reveal new RNA classes and a possible function for pervasive transcription. Science 2007; 316: 1484-8.

33. Gerstein MB, Bruce C, Rozowsky JS, Zheng D, Du J, Korbel JO, Emanuelsson O, Zhang ZD, Weissman S, Snyder M. What is a gene, post-ENCODE? History and updated definition. Genome Res 2007; 17:669-81.

34. Gingeras TR. Origin of phenotypes: genes and transcripts. Genome Res 2007; 17:682-90.

35. Fejes-Toth K, Sotirova V, Sachidanandam R, Assaf G, Hannon GJ, Kapranov P, Foissac S, Willingham AT, Duttagupta R, Dumais E, Gingeras TR. Affymetrix ENCODE Transcriptome Project; Cold Spring Harbor Laboratory ENCODE Transcriptome Project. Post-transcriptional processing generates a diversity of 5'-modified long and short RNAs. Nature 2009; 457: 1028-32.

36. Seila AC, Calabrese JM, Levine SS, Yeo GW, Rahl PB, Flynn RA, Young RA, Sharp PA. Divergent transcription from active promoters. Science 2008; 322: 1849-51.

37. Hirota K, Miyoshi T, Kugou K, Hoffman CS, Shibata T, Ohta K. Stepwise chromatin remodelling by a cascade of transcription initiation of non-coding RNAs. Nature 2008; 456:130–4.

38. Holt SE, Glinsky VV, Ivanova AB, Glinsky GV. Resistance to apoptosis in human cells conferred by telomerase function and telomere stability. Mol Carcinog. 1999; 25: 241-8.

39. Glinsky, GV. Glinskii, AB. Berezovskaya, O. Microarray analysis identifies a death-from-cancer signature predicting therapy failure in patients with multiple types of cancer. J Clin Invest; 2005; 115: 1503 - 1521.

40. Glinsky GV, Higashiyama T, Glinskii AB. Classification of human breast cancer using gene expression profiling as a component of the survival predictor algorithm. Clin Cancer Res. 2004;10: 2272-2283.

41. Glinsky GV, Glinskii AB, Stephenson AJ, Hoffman RM, Gerald WL. Gene expression profiling predicts clinical outcome of prostate cancer. J Clin Invest. 2004;113: 913-923.

42. Glinsky GV, Krones-Herzig A, Glinskii AB, Gebauer G. Microarray analysis of xenograft-derived cancer cell lines representing multiple experimental models of human prostate cancer. Mol Carcinog. 2003;37: 209-221.

43. Tavazoie, S, Hughes, JD, Campbell, MJ, Cho, RJ, Church, GM. Systematic determination of genetic network architecture. Nat. Genet. 1999;22:281-285.

Figure Legends

Figure 1. Constitutive expression of distinct allelic variants of *NLRP1*-locus snpRNAs exerts allele-specific clinically-relevant effects on phenotypes of human cells.

A, THP-1 cells were engineered to stably express distinct allelic variant of the *NLRP1*-locus snpRNAs and induced to differentiate into macrophages. Efficiency of the monocyte/macrophage trans-differentiation was assessed by analysis of viable and apoptotic cells (top panels) and measurements of the number (bottom panels) and phagocytic activity (inset, bottom panel) of macrophages. Note that in response to induction of differentiation, THP-1 cells expressing pathology-linked G-allele snpRNAs undergo massive apoptosis and produce ~ 5-fold less macrophages which are twice less potent in the sheep erythrocyte phagocytosis assay compared to macrophages derived from THP-1 cells expressing ancestral A-allele snpRNAs.

B, Pathology-linked G-allele expressing human fibroblast BJ1 cells manifest significantly higher motility compared to ancestral A-allele expressing BJ1 cells. Gaps of defined distances were created in confluent cultures of BJ1 cells and motility sequences were continuously monitored and recorded using time-lapse video cinematography. For each culture, the initial distance, motility sequence time (time to complete closing of the gap), and motility speed were measured. Average values of six replicate measurements are reported.

C, Human *NLRP1*-locus snpRNAs manifest allele-specific biological activities in mouse macrophages (top left set of bar graphs) and mouse mesenchymal cells (top right set of bar graphs; inset shows results of the similar assay in human mesenchymal cells), which recapitulate the corresponding allele-specific biological activities in human cells. Bottom set of bar graphs shows the biological activities of synthetic 19 nt LNA-oligonucleotide-based structural analogues of the allele-specific variants of NAPL1-locus snpRNAs which were assessed using THP-1 monocyte/macrophages transdiferentiation assays. Note that synthetic LNA-analogues recapitulate the allele-specific patterns of NLRP1-locus snpRNA bioactivities mimicking effects on macrophage numbers (left) and phagocytic activity (right).

Figure 2. Expression of PCS-snpRNAs induces androgen depletion-independent and castration-resistant phenotypes of human prostate cancer.

A. Expression of 8q24 PCS-snpRNAs (red arrows) is induced by *NLRP1*-locus snpRNAs (top gel image), is increased in highly metastatic PC cells and circulating tumor cells (CTC) from orthotopic human PC xenografts (bottom gel images). Prostate cancer susceptibility snpRNAs A6 (rs16901979) manifest increased expression in highly metastatic human prostate carcinoma cells (LNCapLN3, PC3-21) and asserts biologically and clinically-relevant effects on growth of hormone-dependent human prostate carcinoma cells LNCap. RT-PCR analysis demonstrates low expression of prostate cancer susceptibility snpRNAs A6 in normal human prostate epithelial cells RWPE1 and markedly higher expression level in LNCapLN3 cells, which were selected in vivo for increased metastatic potential by serial orthotopic implantation of parental, poorly metastatic LNCap cells. Similarly, expression of multiple PCS-snpRNAs is elevated in blood-borne human prostate carcinoma metastasis precursor cells PC-3-21 compared to the parental cell line PC-3. P values of the corresponding experimental setting versus control experiments are shown.

B, Hormone-dependent human prostate carcinoma LNCap cells engineered to stably express the prostate cancer susceptibility snpRNA A6 acquired ability to survive and grow in androgen-depleted media (set of bars in the top right panel). Note that growth pattern in androgen-depleted media of LNCap cells expressing prostate cancer susceptibility snpRNA allele became similar to highly metastatic LNCapLN3 cells (set of bars in the bottom right panel). Set of bars in the bottom left panel shows the increased survival and growth in androgen-depleted media of LNCap cells constitutively expressing A-alleles of *NLRP1*-locus snpRNAs. Set of bars in the top left panel shows

the results of the Q-PCR analysis of the expression of PCS-snpRNA A6 in RWPE1 normal prostate epithelial cells engineered to stably express distinct allelic variants of the *NLRP1*-locus snpRNAs.

C, Hormone-dependent human prostate carcinoma LNCap cells engineered to stably express the prostate cancer susceptibility snpRNA A6 acquired markedly higher anchorage-independent clonogenic growth potential in agar (top figure) and ability to survive and grow in androgen-depleted media (bottom figure). Note that growth potentials in both agar cultures and androgen-free media of LNCap cells expressing prostate cancer susceptibility A-allele of snpRNA A6 are significantly higher compared to LNCap cells expressing ancestral C-allele. Transfection of anti-sense alleles of PCS-SNP RNA A6 (asA6) diminishes clonogenic growth in agar (inset in top figure) and survival and growth in androgen-depleted media of highly metastatic LNCapLN3 human prostate carcinoma cells (inset in bottom figure).

D. Inoculation of hormone-dependent, low-malignancy human prostate carcinoma LNCap cells engineered to stably express prostate cancer susceptibility snpRNA A6 (LNCap-A6 cells) induces rapidly growing tumors in castrated mice (left figures). Note that tumors in castrates appear larger and growing faster compared to the sham-operated mice (right figures). No tumors were detected in either castrate or shame-operated groups within the indicated observation periods after inoculation of parental or control-transfected LNCap (insets). Bottom set of figures show images of cultured in vitro in androgen-depleted media of LNCap-A6 cells which were recovered from tumors in castrated mice.

Figure 3. Increased expression of *NLRP1*-locus snpRNAs and PCS-snpRNA A6 in clinical prostate carcinoma samples.

A, B, Q-PCR analysis reveals markedly increased expression of *NLRP1*-locus snpRNAs (A) and PCS-snpRNA A6 (B) in clinical PC samples compared to adjacent normal prostate (far left set of

bars in each panel). Note the apparent correlation of the expression levels with the stage (top panels) and Gleason scores (bottom panels). Each data set is shown in two different scales to account for markedly distinct PCS-snpRNA expression levels in different group of samples. Each bar shows the actin-normalized value of the expression level of corresponding snpRNAs in samples from individual patients as determined by the Q-PCR analysis. Shaded areas highlight the thresholds of expression levels exceeding 99% confidence intervals defined by the expression levels in adjacent normal prostate samples. 48 pathologist-verified clinical samples of the OriGene TissueScan Cancer qPCR Arrays Prostate Cancer Panel III were analyzed in accordance with the supplier's protocols. QC data, pathology reports, and associated clinical information are available at http://www.origene.com/qPCR/Tissue-qPCR-Arrays.aspx.

C, Correlation plots and linear regression analyses documenting reproducibility of technical replicates of the Q-PCR analysis of the expression levels of PCS-snpRNA A6 (top left figure; $r = 0.899$; $p < 0.0001$) and *NLRP1*-locus snpRNA (top right figure; $r = 0.942$; $p < 0.0001$). Bottom left figure illustrates highly significant correlation of the expression of *NLRP1*-locus snpRNA and PCS-snpRNA A6 in prostate tumor samples from patients diagnosed with prostate adenocarcinoma ($r = 0.896$; $p < 0.0001$). Bottom right figure shows the average expression values of the PCS-snpRNA A6 and *NLRP1*-locus snpRNA in adjacent normal prostate samples and prostate cancer samples from tumors with different Gleason scores. Note markedly higher average expression levels of snpRNAs in tumor samples with high Gleason scores and increasing proportion of patients in high Gleason score groups with snpRNA expression levels exceeding thresholds of 99% confidence interval defined by the expression levels in adjacent normal prostate samples. Inset illustrates these relationships within the 400X scale of fold expression changes normalized to the average expression values in adjacent normal prostate samples.

Figure 4. Identification and characterization of genomic trans-regulatory domains (GTRDs) which are located in intergenic disease-associated genetic loci (IDAGL), manifest enhancer/insulator activities, and transcribe biologically active snpRNAs.

A. Chromatin state map analysis of the intergenic disease-associated genomic region transcribing *NLRP1*-locus snpRNA rs2670660. Boxed areas depict the locations of the *NLRP1* promoter (red box) and two intergenic enhancers (blue boxes), one of which is characterized in this study and shown at higher resolution in the bottom figure. Positions of disease-linked SNP nucleotides within snpRNA-encoding sequences are indicated by vertical lines. Chromatin state maps of individual snpRNA-encoding genomic sequences in human embryonic stem cells are visualized using the custom tracks of the UCSC Genome Browser (http://genome.ucsc.edu/ENCODE/). Color-coded horizontal lines depict alignments of DNA sequences derived from Chip-Seq experiments using antibodies against corresponding proteins. Individual zoom-in chromatin state maps aligned to corresponding snpRNA-encoding sequences are shown with the corresponding disease-linked SNPs (Supplemental Figures 2-4). Original experiments describing the corresponding mouse and human genome-wide chromatin state maps were reported elsewhere (6).

B. Luciferase reported assay reveals allele-specific enhancer/insulator activities of the 2 kb intergenic DNA sequence containing distinct allelic variants of the rs2670660 *NLRP1*-locus SNP. Luciferase reporter assay to assess the enhancer activity of 2 kb *NLRP1*-locus intergenic region was carried out in RWPE1 (set of bars in left top panel) and HEK293 set of (set of bars in the right top panel) cells transiently expressing either control luciferase reporter plasmids or plasmids containing chemically synthesized 2 kb sequences flanking distinct allelic variants of the *NLRP1*-locus integenic SNP rs2670660, which is positioned exactly in the middle of the enhancer's sequence. Note decreased enhancer's and insulator's activities in ancestral A-allele constructs compared to pathology-linked G-allele constructs. Bottom panels of bars show the effects of *NLRP1*-locus

snpRNAs on enhancer and insulator activities in RWPE1 cells. Note that distinct alleles of the *NLRP1*-locus intergenic enhancer manifest different responses to the *NLRP1*-locus snpRNAs: enhancer's activities in ancestral A-allele constructs are completely blocked compared to pathology-linked G-allele constructs.

C. Molecular anatomy of the network of intergenic long-range enhancers (iLREs) and snpRNAs facilitating castration-resistant phenotype of human prostate cancer. *NLRP1*-locus snpRNAs, which are transcribed from the intergenic long-range enhancer sequence located in 17p13 region at ~ 30 kb distance from the *NLRP1* gene, regulate expression level of 8q24-locus PC susceptibility snpRNAs (bottom gel images and Figure 2), which are transcribed from intergenic enhancers located in the prostate cancer susceptibility regions 1, 2, and 3 (middle figures). Activity of the iLRE containing PCS SNP rs6983267 is increased 15-20-fold by the co-transfection of beta-catenin/TCF4 transcription factors, expression of which is significantly elevated in RWPE1 cells engineered to constitutively express *NLRP1*-locus snpRNAs (sets of bars in inset). In contrast, expression of antagonists of beta-catenin, *DACT3* and *DCAT1*, is decreased in *NLRP1*-locus snpRNA-expressing cells. References to the original publications reporting chromatin state maps, activity of intergenic enhancers, and identification of trans-regualtory snpRNAs of the 8q24 prostate cancer susceptibility regions 1, 2, and 3 are indicated and discussed in the main text.

D. Graphical representations of the reported in the Supplemental Table S10 and Supplemental Figure S4 chromatin state maps of 43 IDAGLs. Areas highlighted in red and blue indicate disease-type-specific transcription factor signatures which appear associated with sets of pathogenetically- and/or epidemiologically-related disorders. Each column represents the individual IDAGL containing an SNP associated with a particular trait or disease phenotype. Each row corresponds to the individual chromatin state marker protein. Last row shows a cumulative chromatin state score

indicating how many proteins were bound in close proximity of the corresponding SNPs. Visualization and links to original experimental data are publicly available (http://genome.ucsc.edu/ENCODE/).

Figure 5. snpRNA sequences represent allele-specific “decoy” targets of microRNAs which function as SNP-allele-specific enhancers of microRNA expression and activity.

A - E. Experimental evidence and computational analysis supporting the allele affinity model of snpRNA-mediated regulation of microRNA expression and activity.

A. ABI TaqMan PCR-based screen identifies a statistically significant set of 36 microRNAs expression of which is altered at least 1.5-fold in *NLRP1*-locus snpRNA-expressing cells compared to control BJ1/EGFP cells and differentially regulated in pathology-linked G-allele-expressing BJ1 cells compared to the ancestral A-allele-expressing cells (set of bars in the top left panel). Note that 18 of 36 (50%) of these microRNAs are derived from the single microRNA cluster on ~ 200 kb continuous region of 14q32 band of chromosome 14, which suggest that 14q32 cluster microRNAs may be primary molecular targets of the *NLRP1*-locus snpRNAs (Supplemental Figure S6). Microarray analysis of human BJ1 cells engineered to stably express distinct allelic variants of the NLRP1-locus transRNAs reveals allele-specific alterations of expression levels of multiple distinct classes of non-coding RNAs which include snoRNAs and snoRNA-host genes (SNORD113; SNHG1; SNHG3; SNHG8), long non-coding RNAs (MEG3, tncRNA, HOTAIR, and MALAT1), microRNAs, microRNA-precursors, and protein-coding microRNA-host genes (ATAD2; KIAA1199). Note that changes of expression of intron-residing microRNAs miR-548d (intron of the ATAD2 gene) and miR-549 (intron of the KIAA1199 gene) are in good correspondence with allele-specific expression levels of corresponding microRNA-host genes which suggest a coordinated mechanism of regulation (Supplemental Figure S6).

A-D, Expression of high affinity (low mfe) snpRNA alleles in human cells (defined by allele-specific changes in minimal free energy (mfe) of snpRNA/microRNA hybridization) is associated with increase in abundance levels of corresponding microRNAs. A, Statistically highly significant inverse correlation between allele-specific changes in minimal free energy (mfe) of snpRNA/microRNA hybridization and experimentally-defined changes of microRNA expression that is lower mfe values correspond to higher levels of microRNA expression (A, set of bars in the top right panel). These relationships are shown for individual microRNAs the abundance levels of which in human cells are induced (miR-302a; miR-629; miR-548d; miR-126; miR-770-5p; Figure B) or repressed (miR-20b; let-7b; miR-133a; miR-205; Figure C) by forced expression of pathology-linked G-allele snpRNAs compared to ancestral A-allele-expressing cells. Inset bars show the results of Q-PCR analysis of expression of corresponding microRNAs (see additional analysis and examples in the Supplement and Supplemental Figure S8).

E, Expression of *NLRP1*-locus snpRNAs in human cells induces allele-sequence-dependent changes in expression (top sets of bars) and activity (bottom sets of bars) of microRNAs. Q-PCR measurements of the expression levels and luciferase reporter assay of miR-205 and let-7b activities in RWPE1 cells stably expressing distinct allelic variants of the *NLRP1*-locus snpRNAs demonstrates significant changes of expression and activity of both microRNAs in high affinity (A-allele) snpRNA-expressing cells compared to low affinity (G-allele) snpRNA-allele-expressing cells.

Figure 6. Regulatory cross-talk between *NLRP1*-locus snpRNAs, 8q24-locus PCS-snpRNAs, and snpRNA-regulated microRNAs induces similar clinically-relevant phenotypes in human cells.

A, Q-PCR analysis of microRNA expression in human cells engineered to constitutive express *NLRP1*-locus snpRNAs identifies concordant SNP-allele-sequence-specific changes of expression

levels of three microRNAs, miR-375, miR-20b, miR-205 expression of which increased in human embryonic stem cells and blood-borne human prostate carcinoma metastasis precursor cells (Supplemental Figure S10). Human cell lines engineered to constitutive express *NLRP1*-locus snpRNAs manifest altered expression profiles of PCS-snpRNAs (Figure 2; induced PCS-snpRNAs are marked with red arrows) and expression levels of three stemness microRNA (miR-375, miR-20b, miR-205).

A-B, Human cells engineered to constitutive express *NLRP1*-locus snpRNA-regulated stemness microRNAs (miR-375, miR-20b, miR-205) manifest dramatic changes of anchorage-independent growth in agar (RWPE1 cells; Figure A, bottom panel) and clonogenic growth potential in clonogenicity assays (BJ1 cells; Figure B). These microRNA-induced phenotypic changes recapitulate phenotypes of human cells engineered to constitutively express *NLRP1*-locus snpRNAs and PCS-snpRNAs (Figures 1 & 2; Supplemental Figure S9; and ref. 4).

C-E, Microarray analysis reveals activation of snpRNAs/miR-205 axis in human prostate cancer. Microarray expression profiling experiments identify a set of 47 transcripts manifesting highly concordant expression profiles ($r = 0.705$; $P < 0.0001$) in RWPE1 human prostate carcinoma cells engineered to stably express either microRNA miR-205 or *NLRP1*-locus snpRNAs, in blood-borne human prostate carcinoma metastasis precursor cells of PC3 lineage, and in highly metastatic variants (LNCapLN3; LNCap-C4-2; LNCap-C4-2B) of LNCap lineage (C).

D, Refinement of the 47-transcript signature to yield individual Pearson correlation coefficients > 0.5 in highly metastatic cell lines and < - 0.6 in parental and less metastatic variant LNCapPro5 (top sets of bars) generates the 30-gene expression signature which manifest highly concordant expression profiles in clinical samples of distant metastatic lesions (bottom sets of bars) compared to normal prostate samples ($p = 1.1E-11$), histologically normal prostate tissue samples adjacent to

tumors (p = 5.1E-21), and primary prostate tumors (p = 3.0E-18). Multivariate Cox regression analysis of the 30 genes comprising the miR-205 signature identifies highly significant 16-gene therapy failure prediction model (Chi Square = 47.1919; p = 0.0001); Kaplan-Meyer analysis of clinical samples from 79 prostate cancer patients with known clinical outcomes after radical prostatectomy (39, 41) using weighted survival prediction algorithm (39) demonstrates that patients with distinct expression profiles of the 16-gene miR-205 signature have statistically distinct probability of therapy failure (Log rank test: Chi Square = 64.67; p < 0.0001; Figure E). Note that all patients (100%) in the top quartile failed therapy; in contrast, only 16% of patients in the bottom quartile failed therapy within 5 years after radical prostatectomy.

Figure 1.

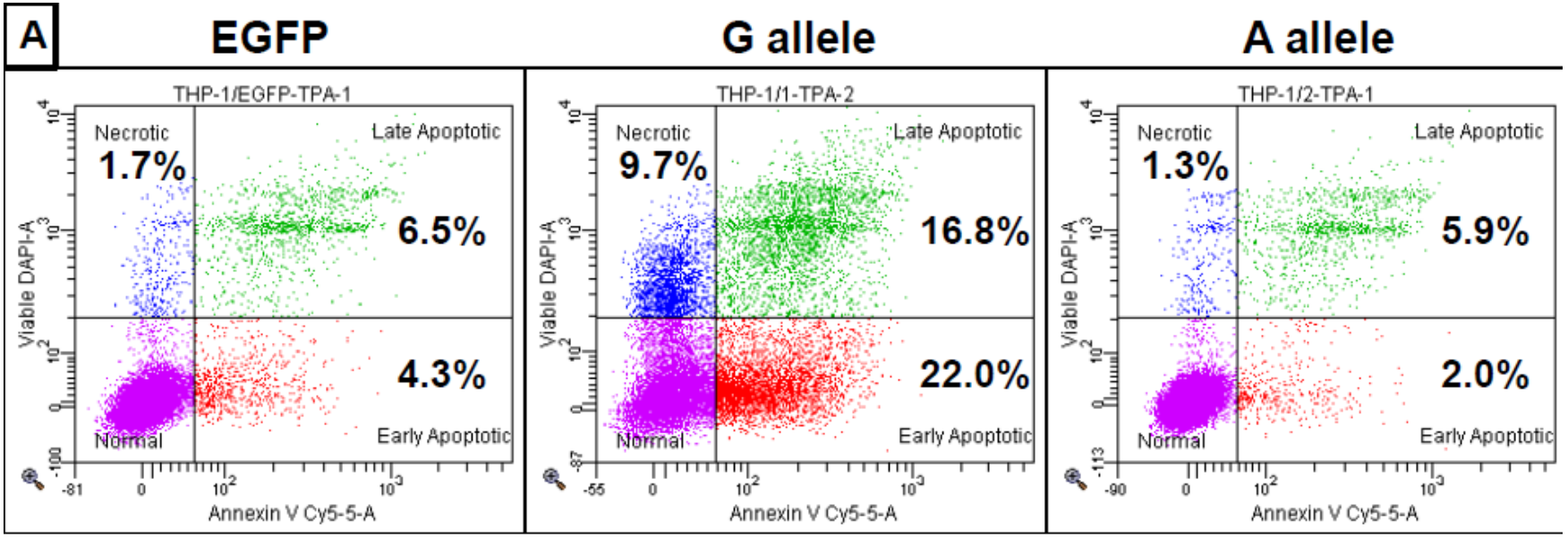

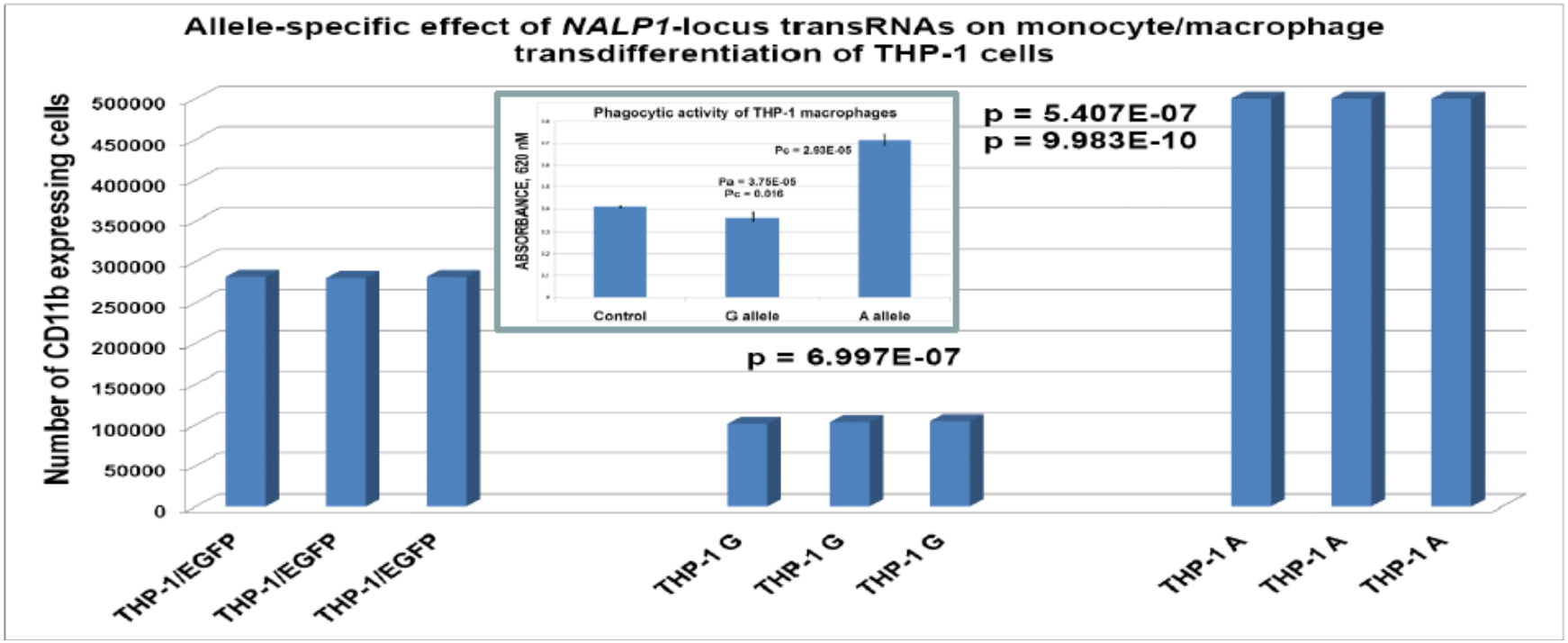

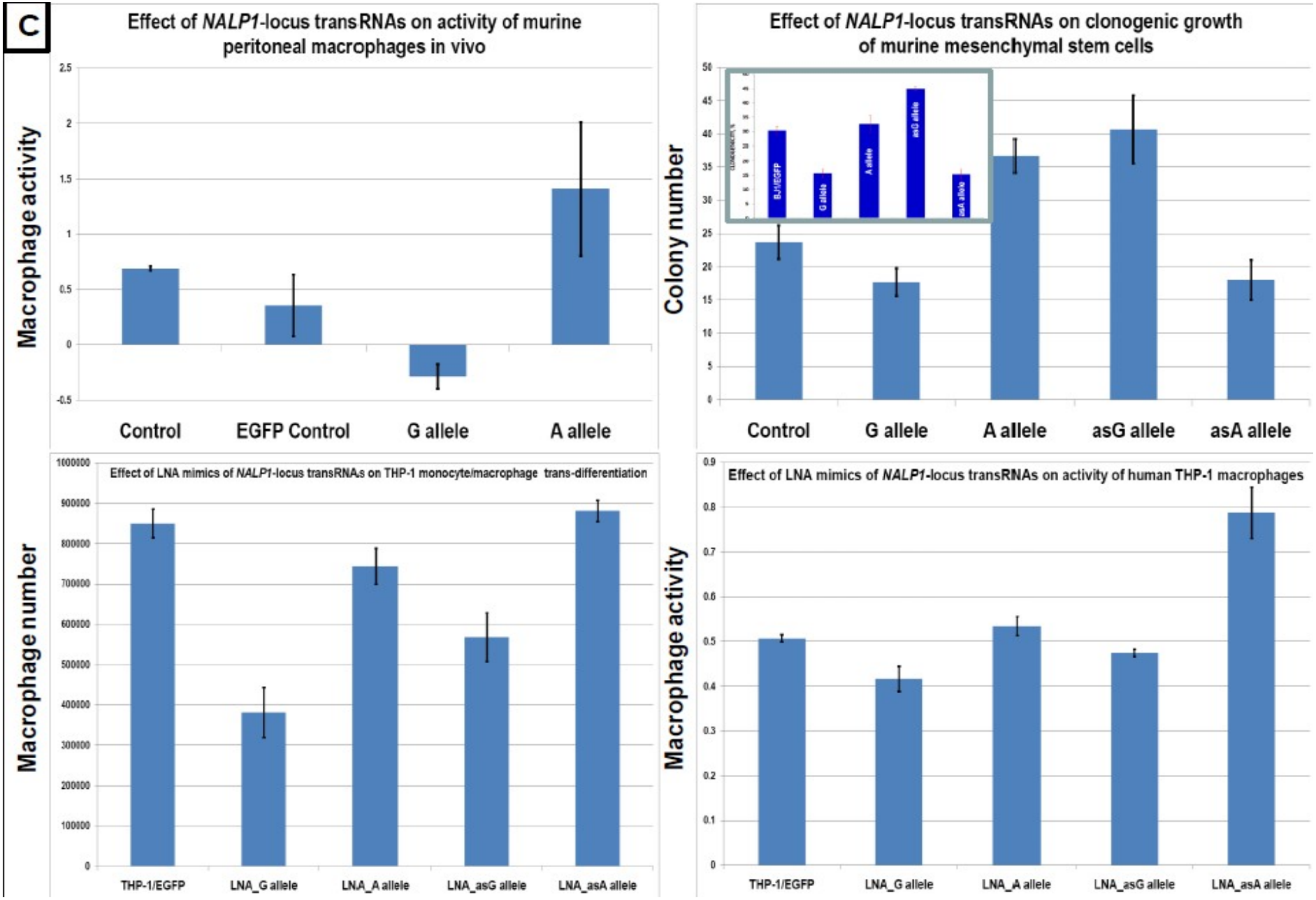

Figure 2.

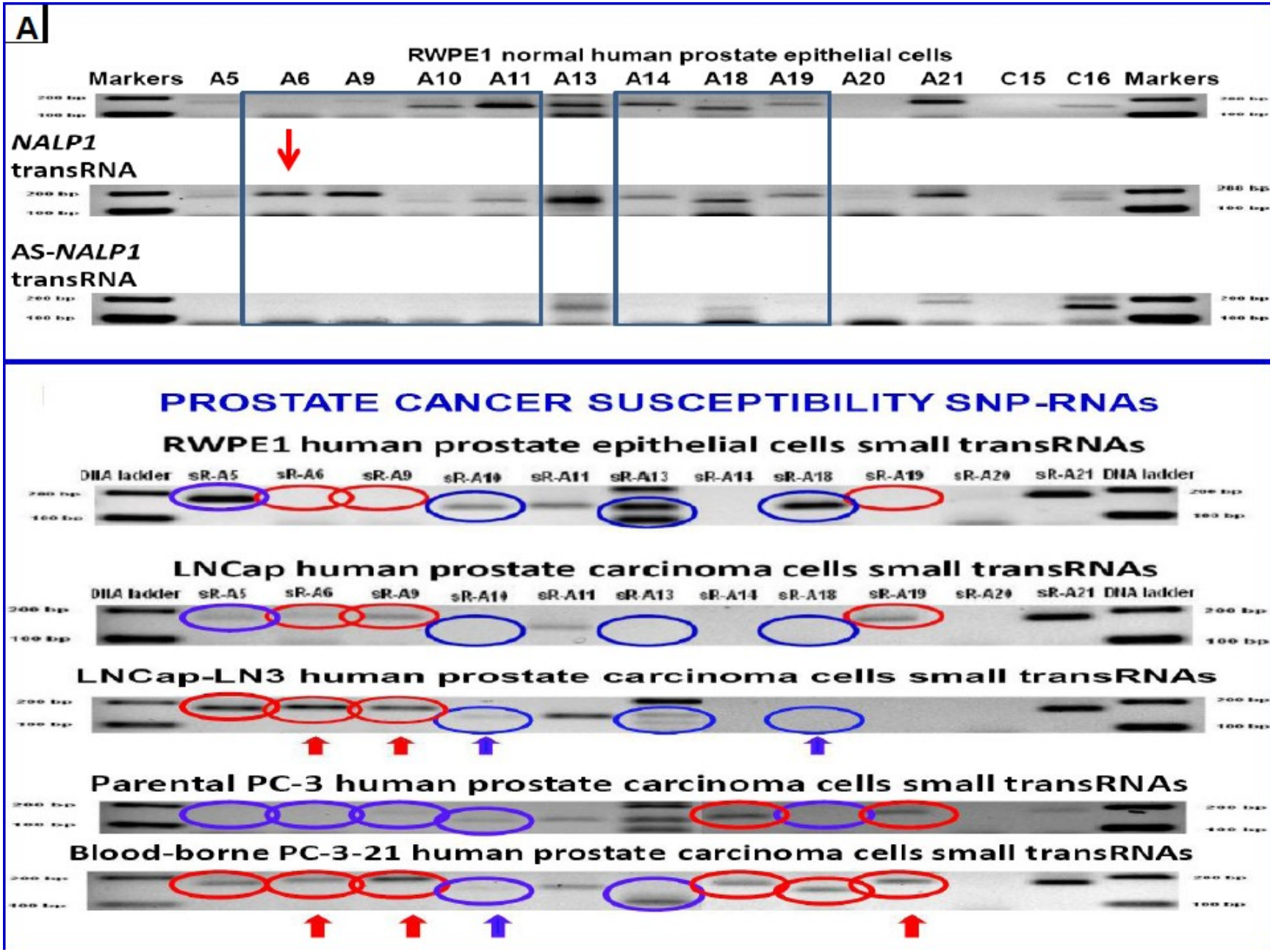

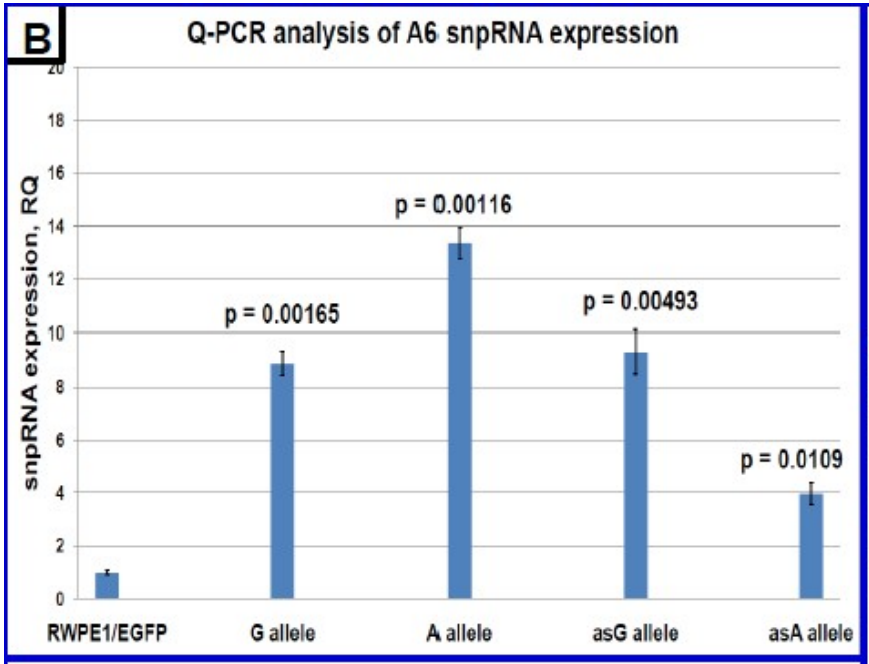

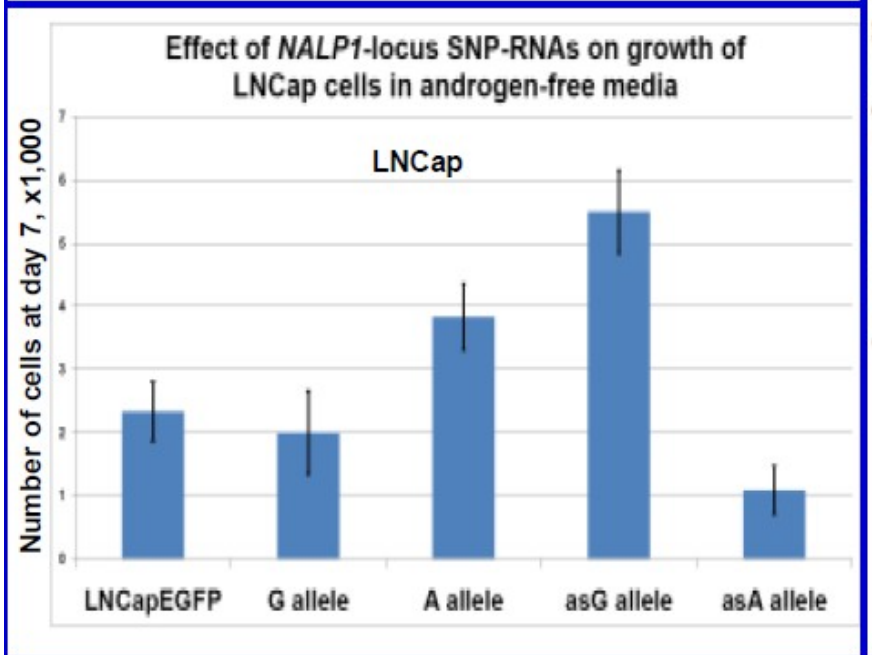

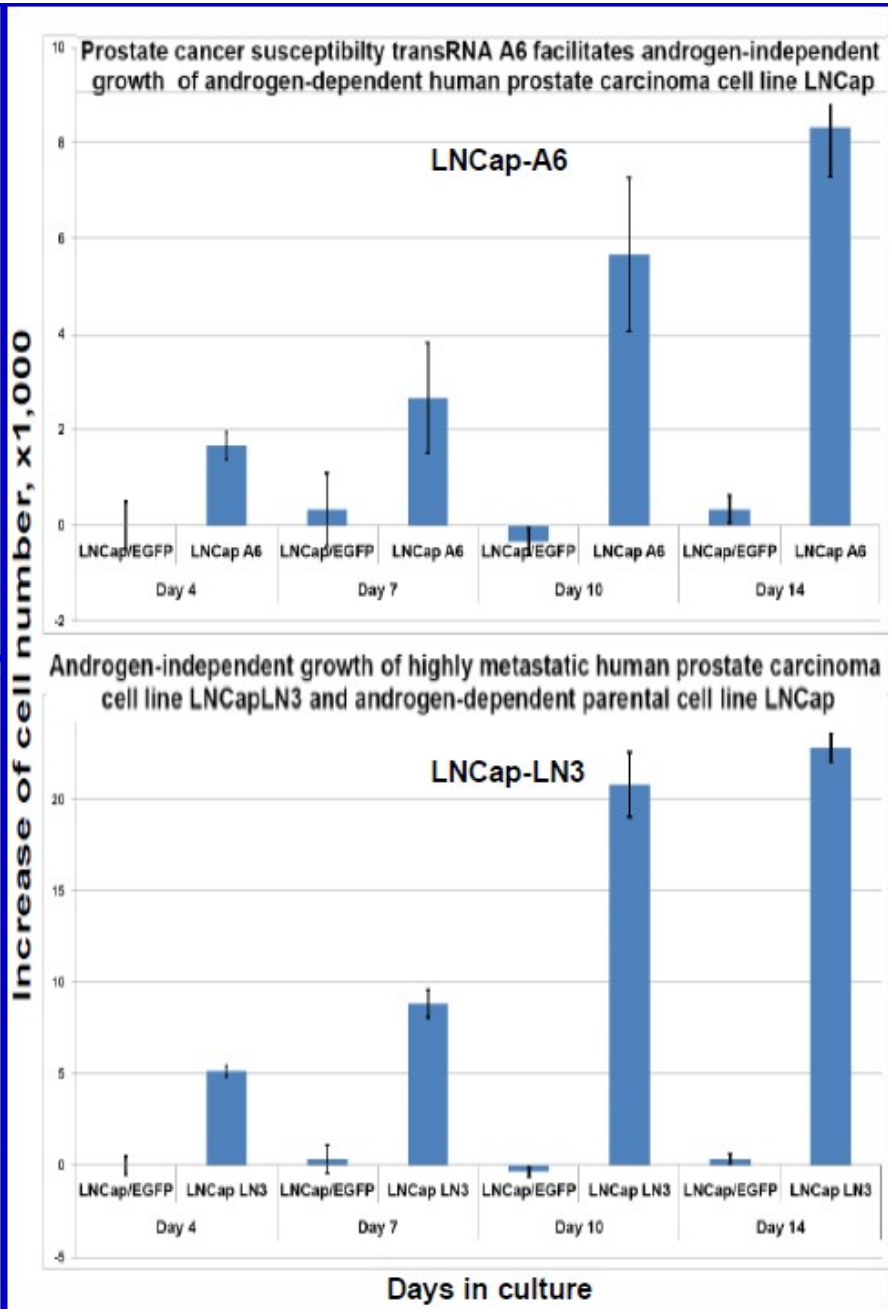

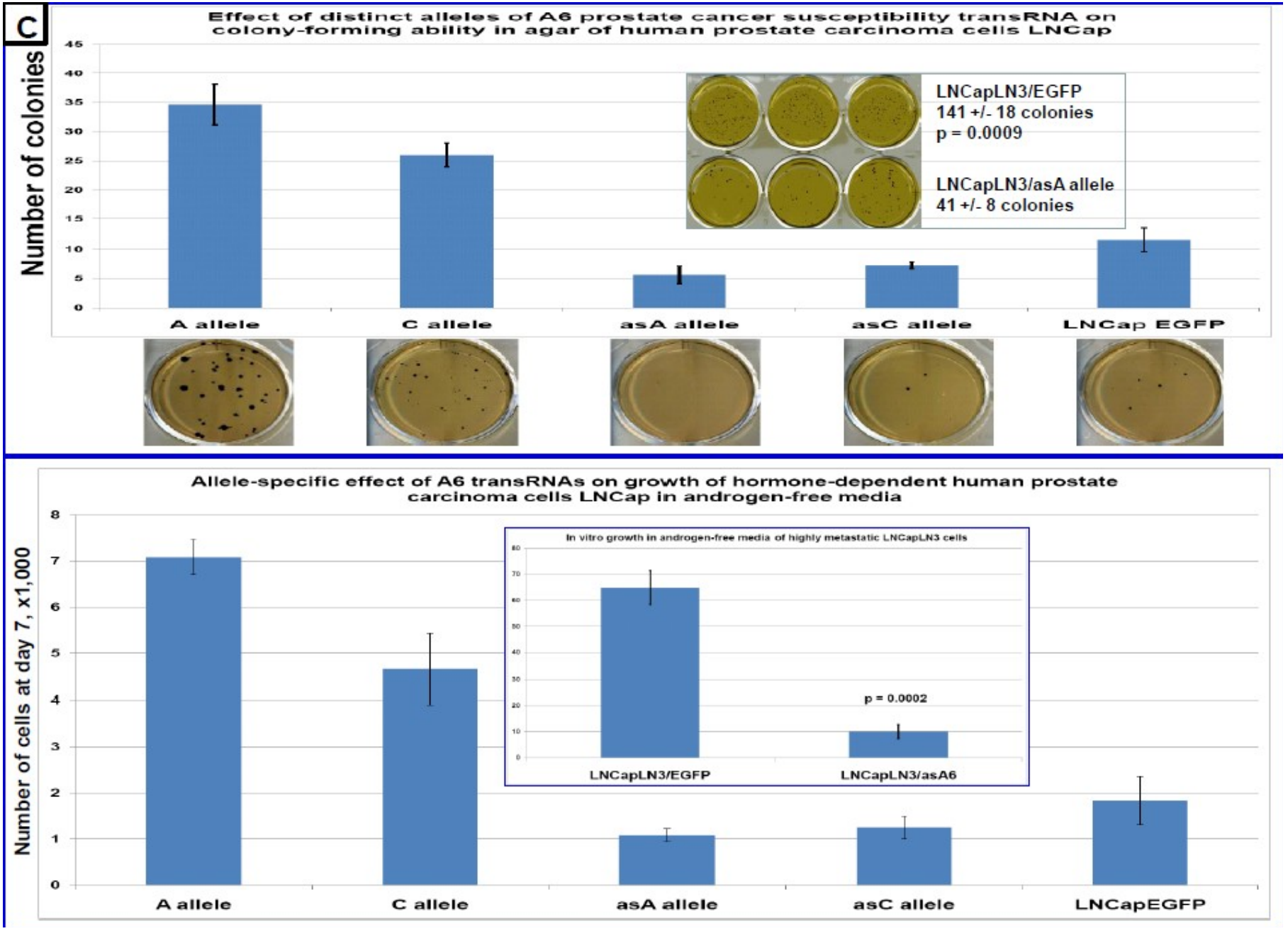

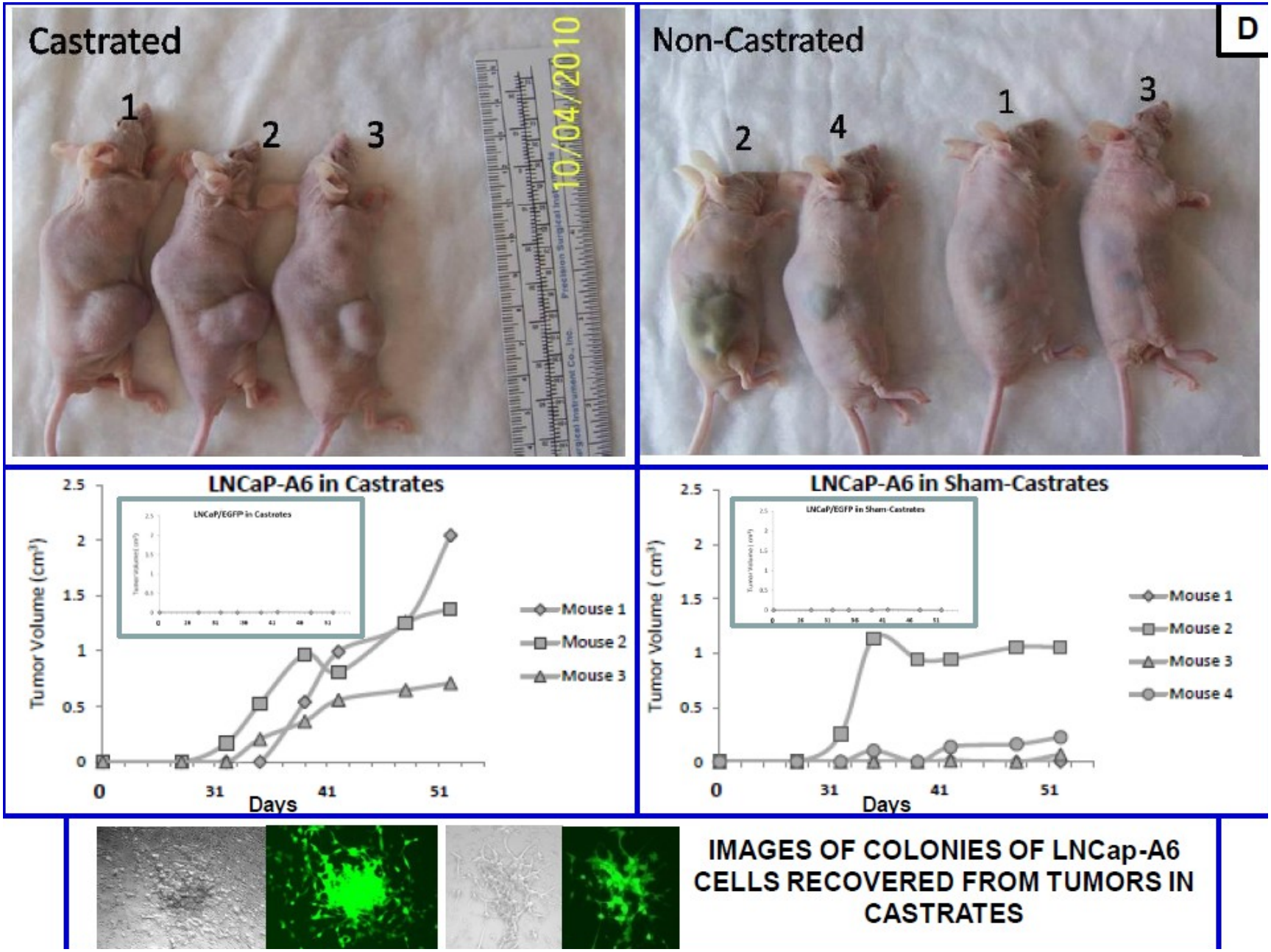

Figure 3.

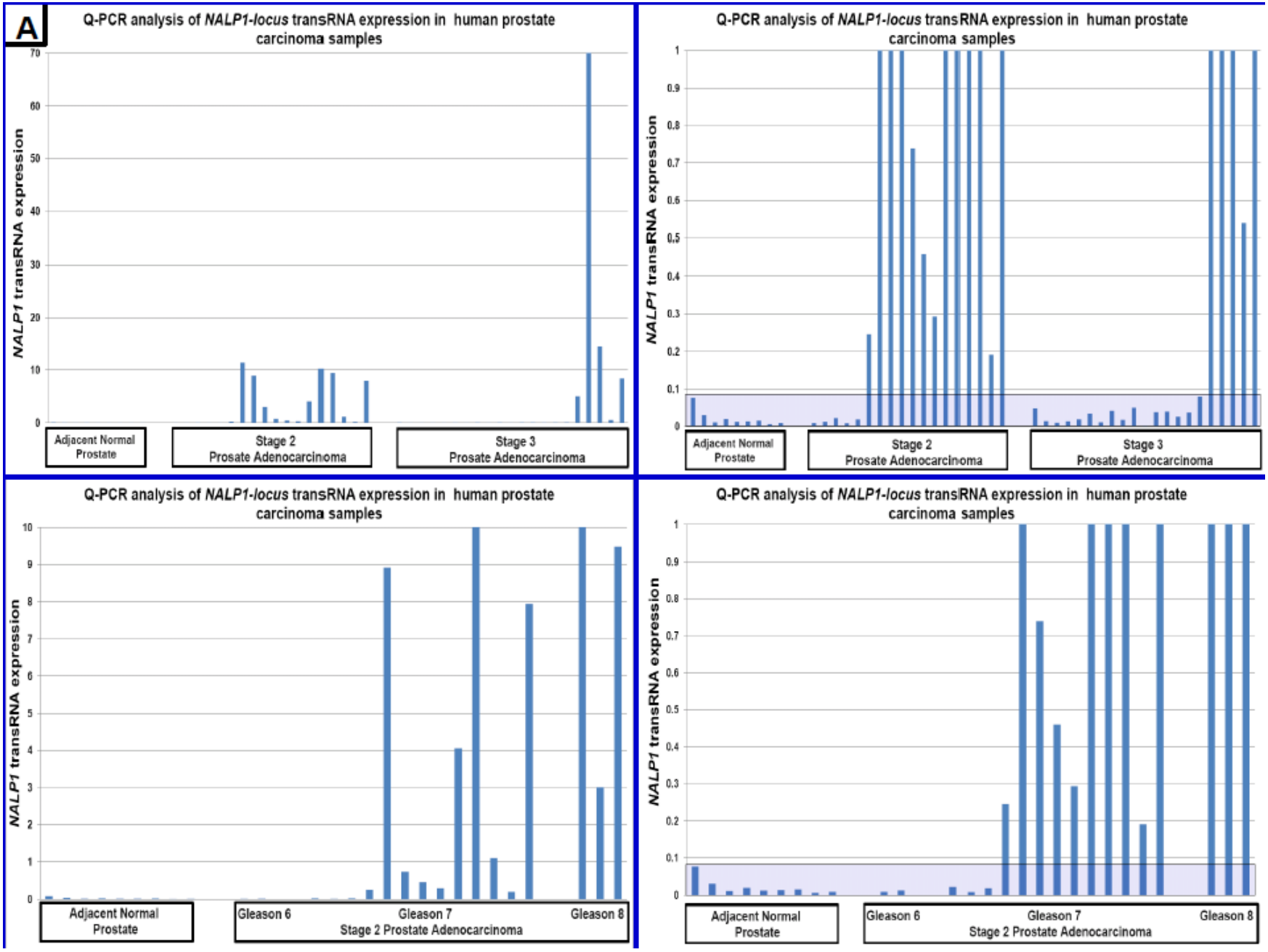

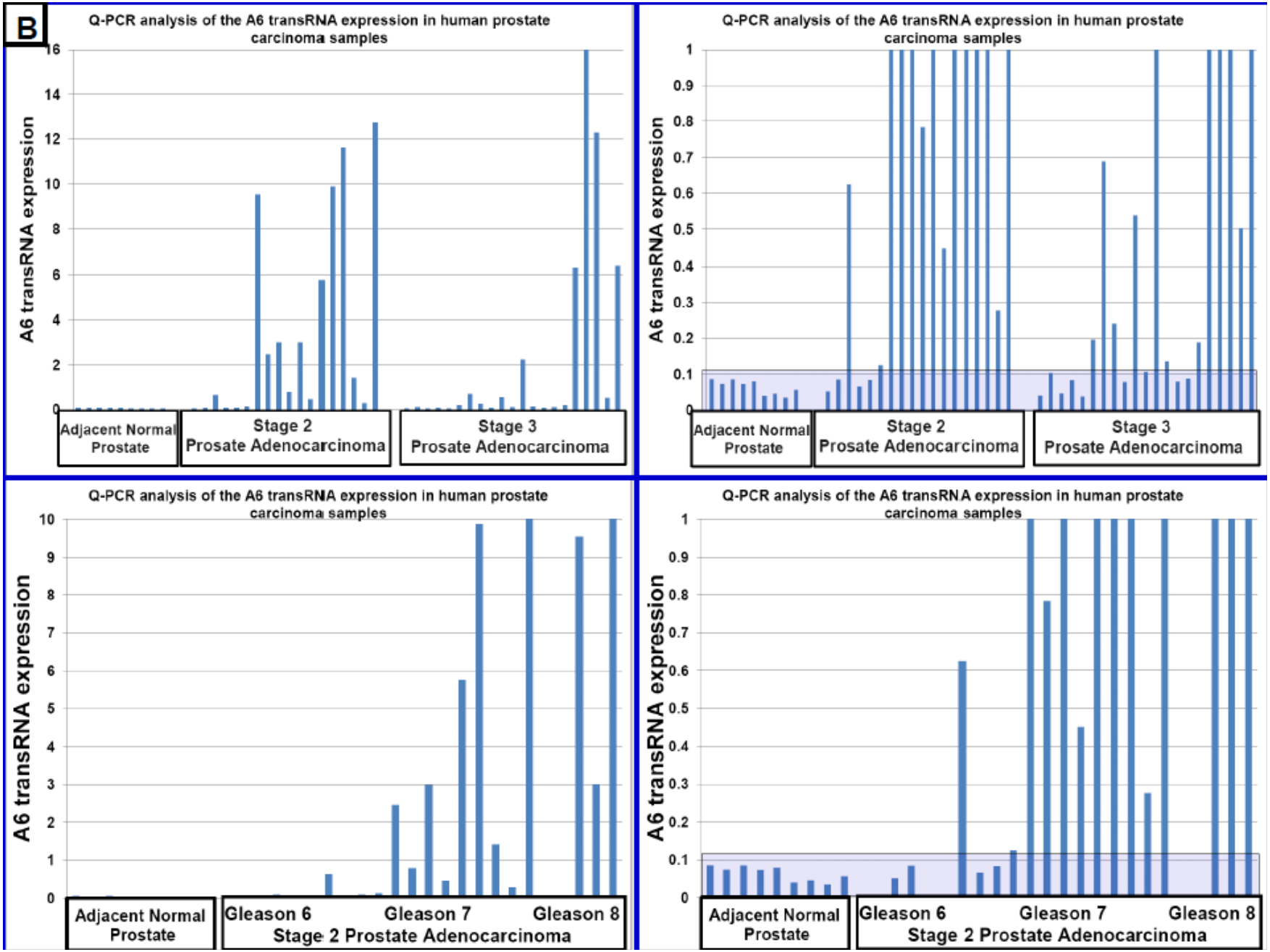

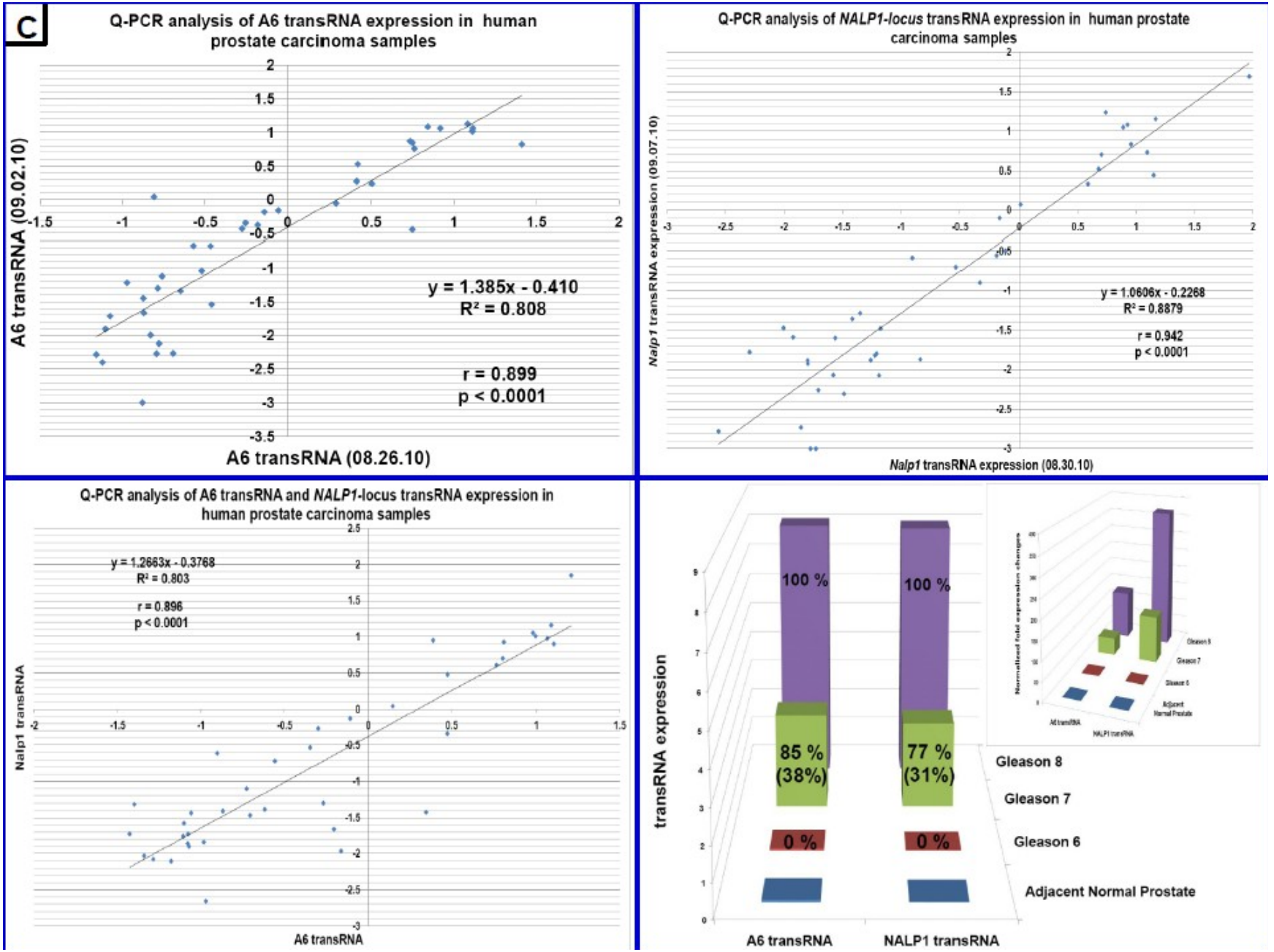

Figure 4.

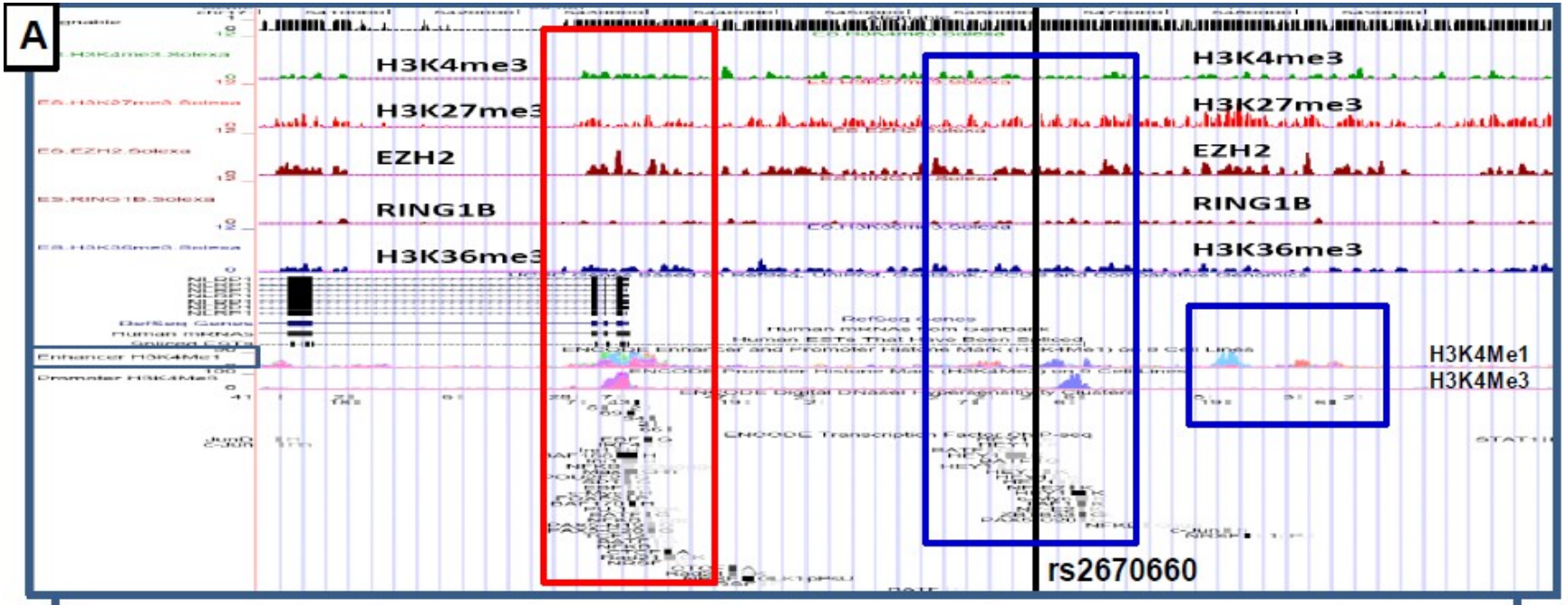

NALP1-locus promoter and enhancers
chr17:5,400,000-5,500,000

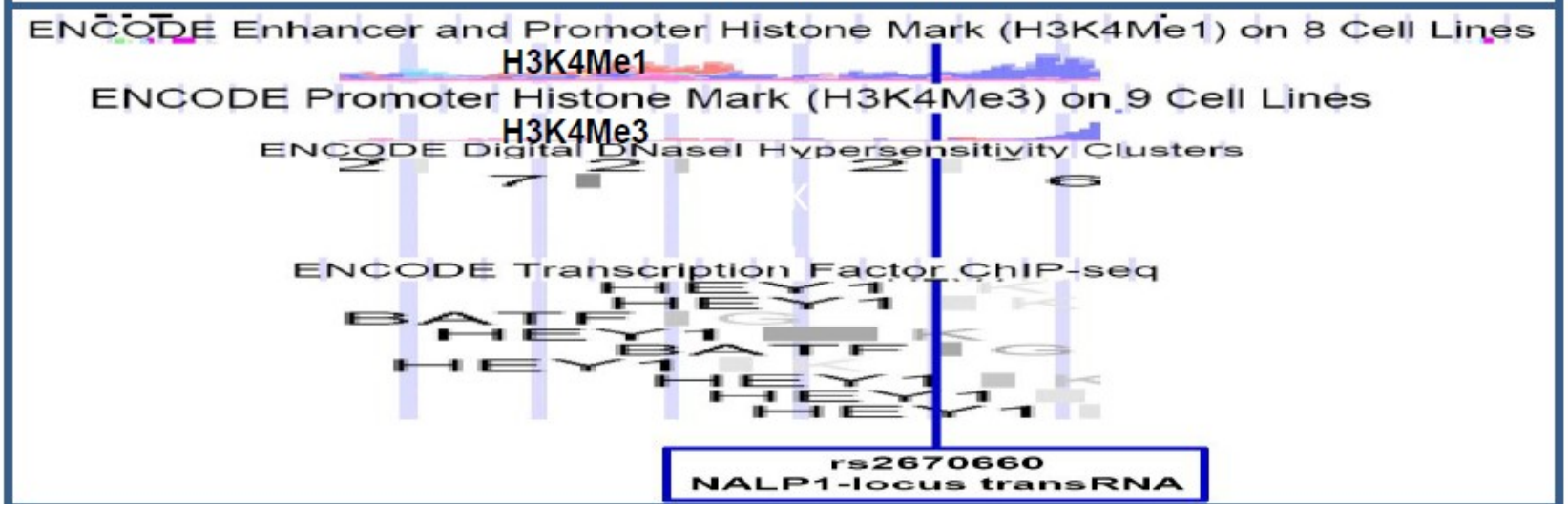

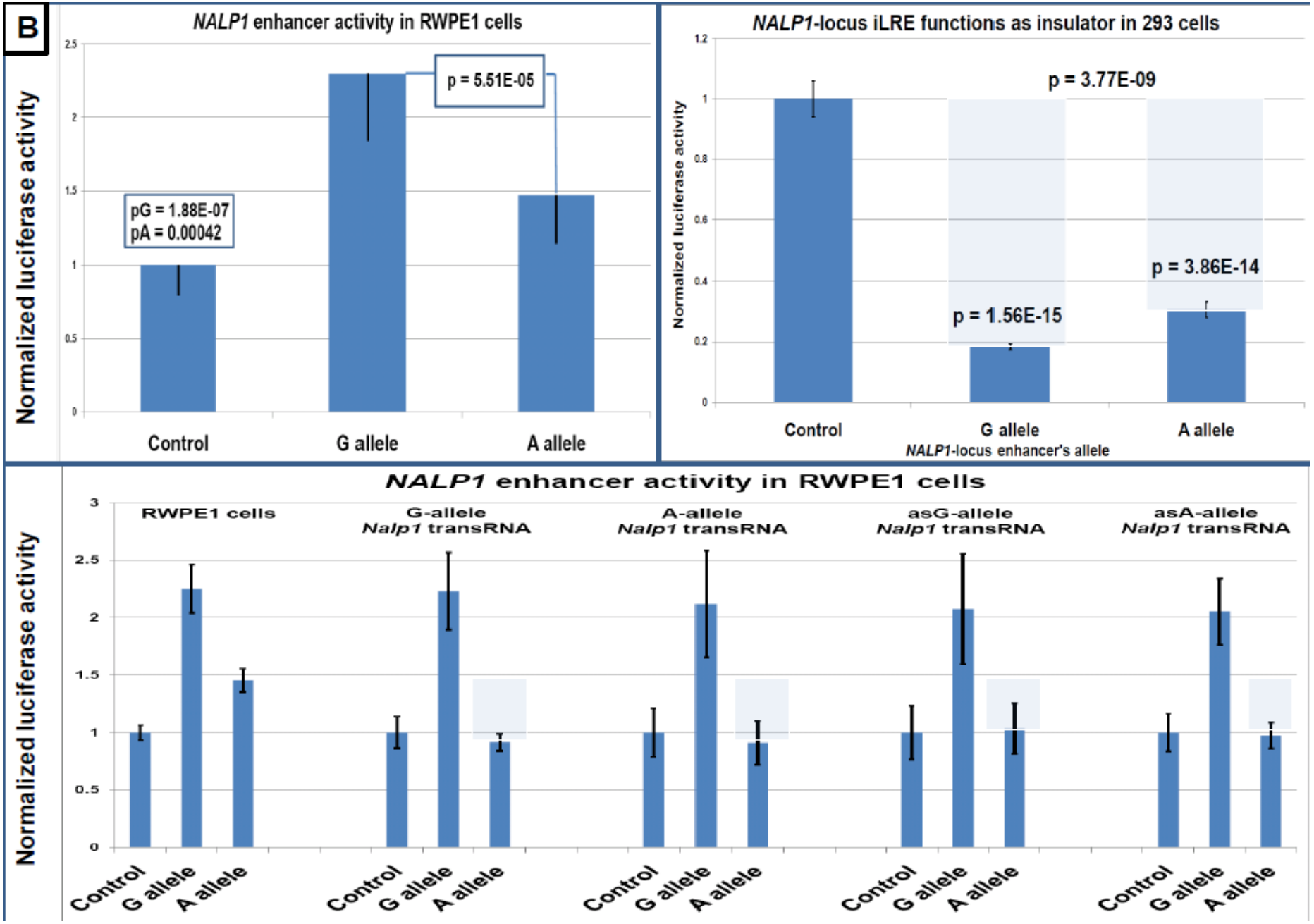

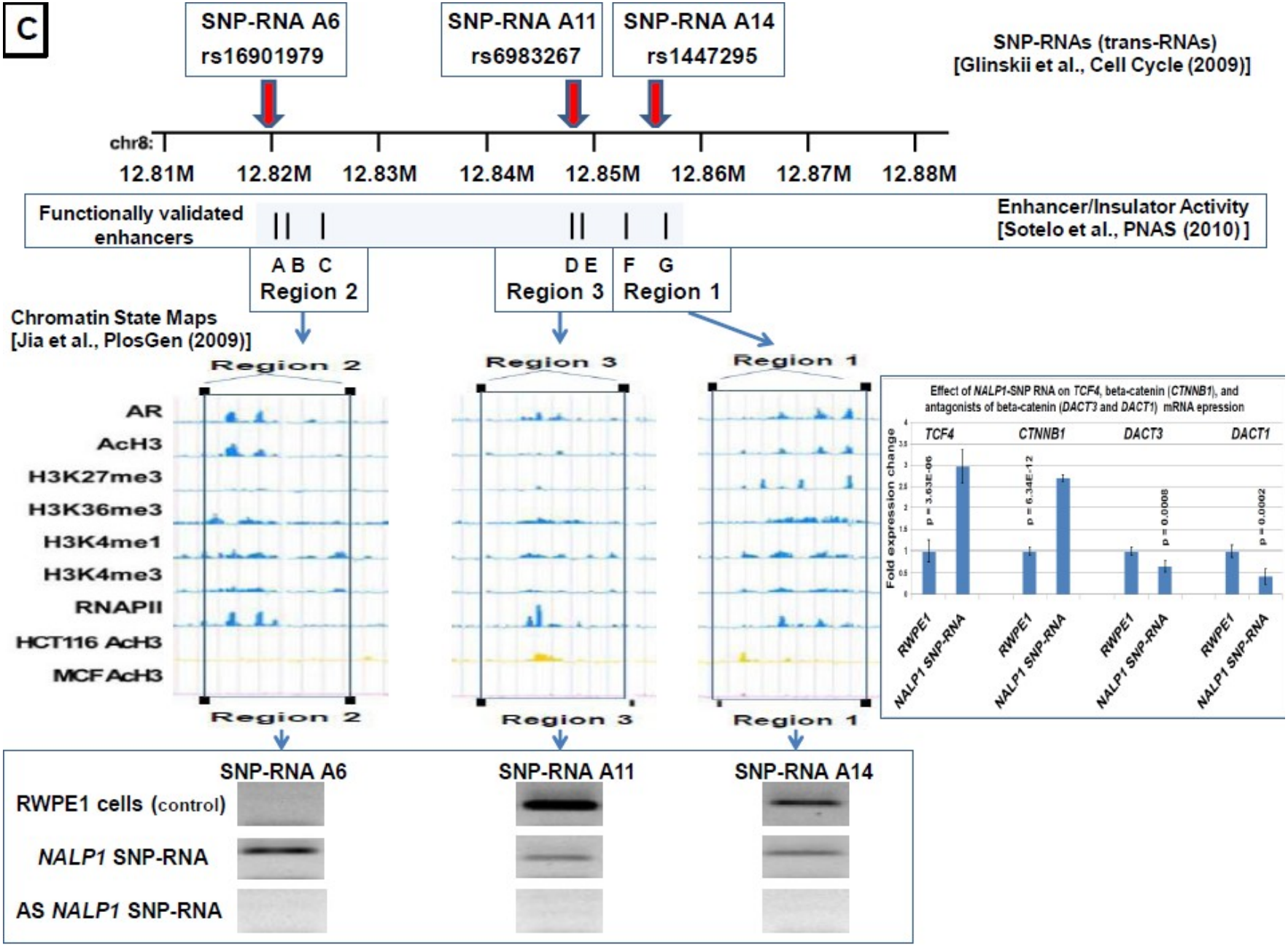

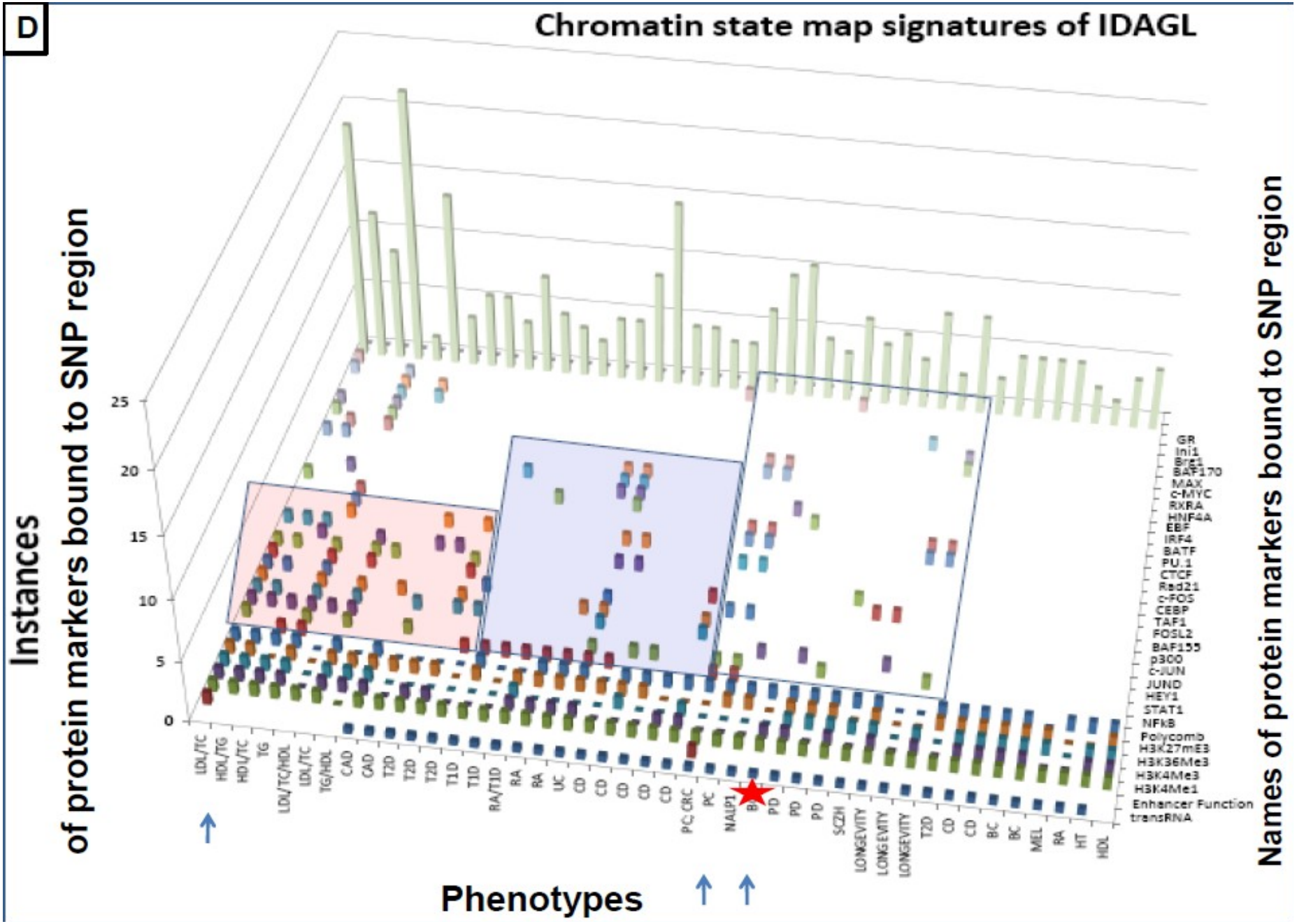

Figure 5.

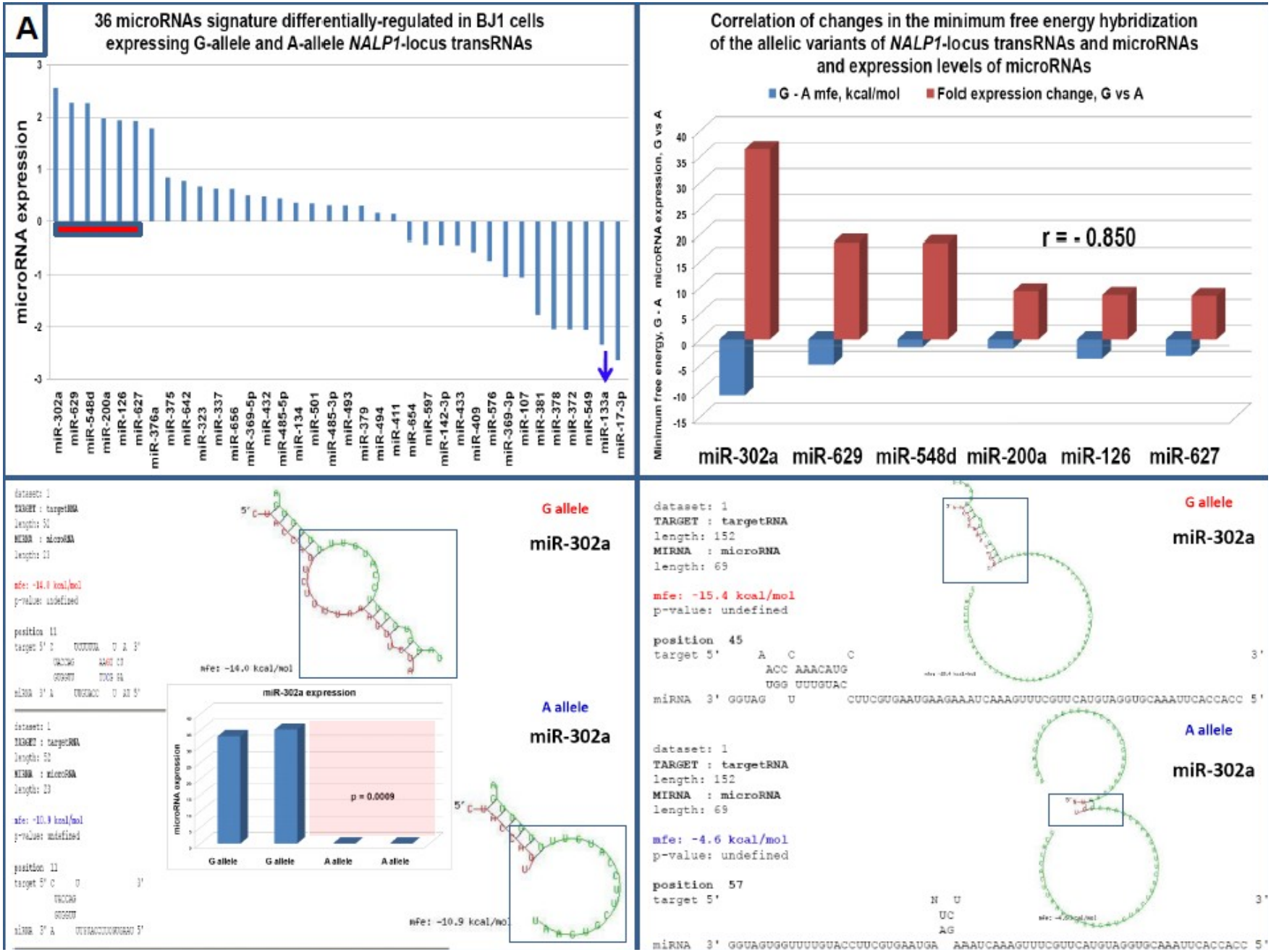

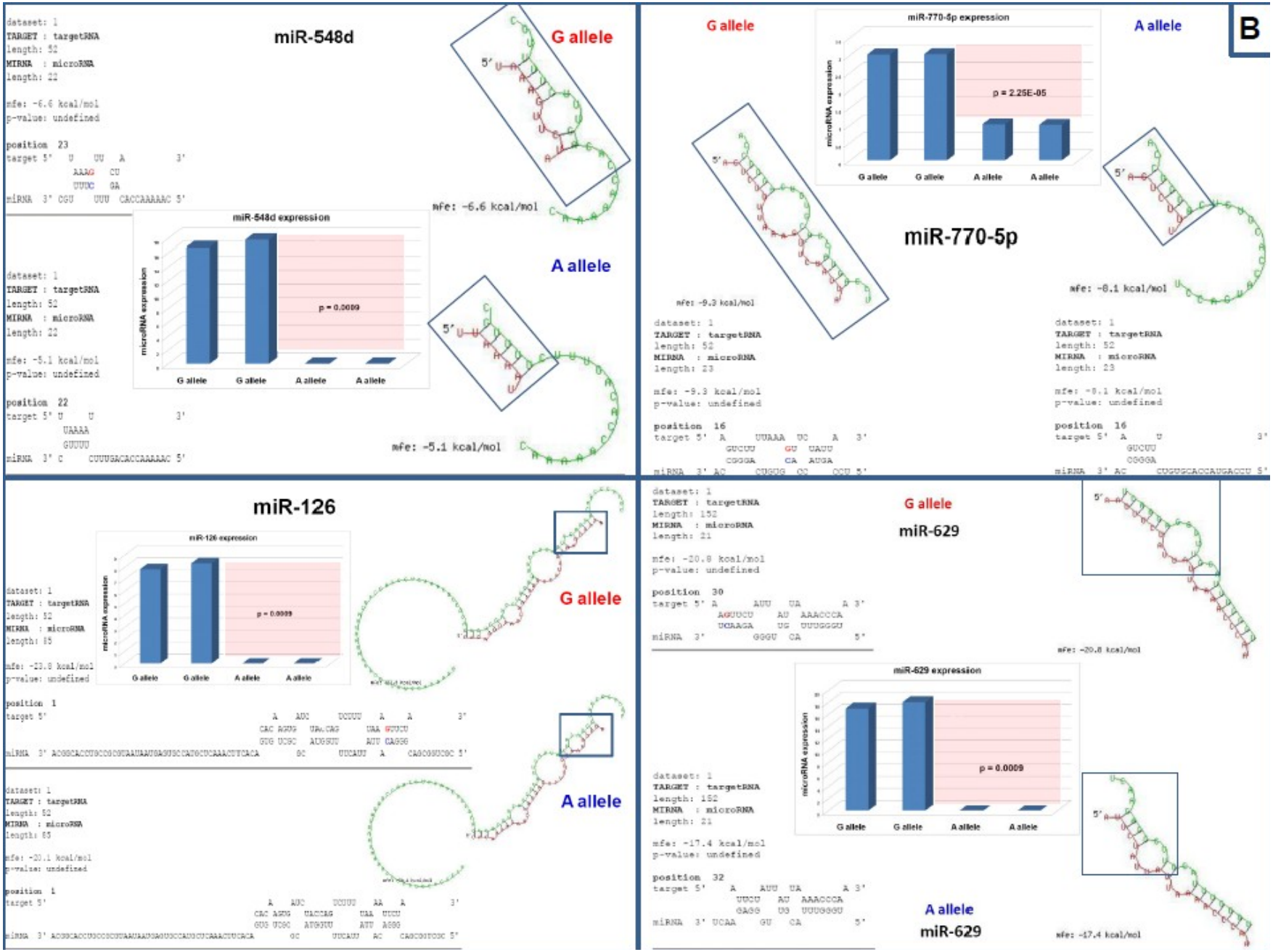

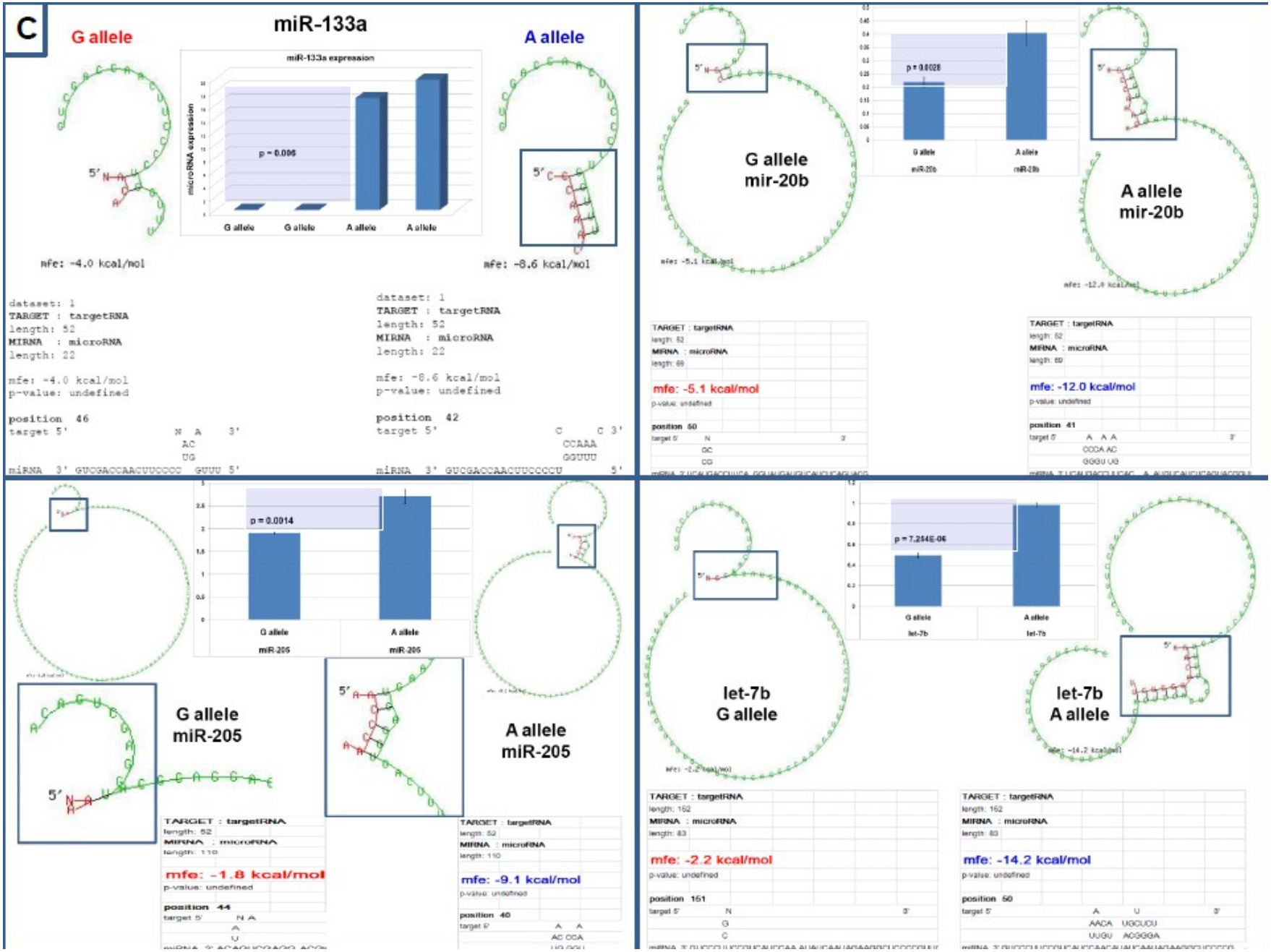

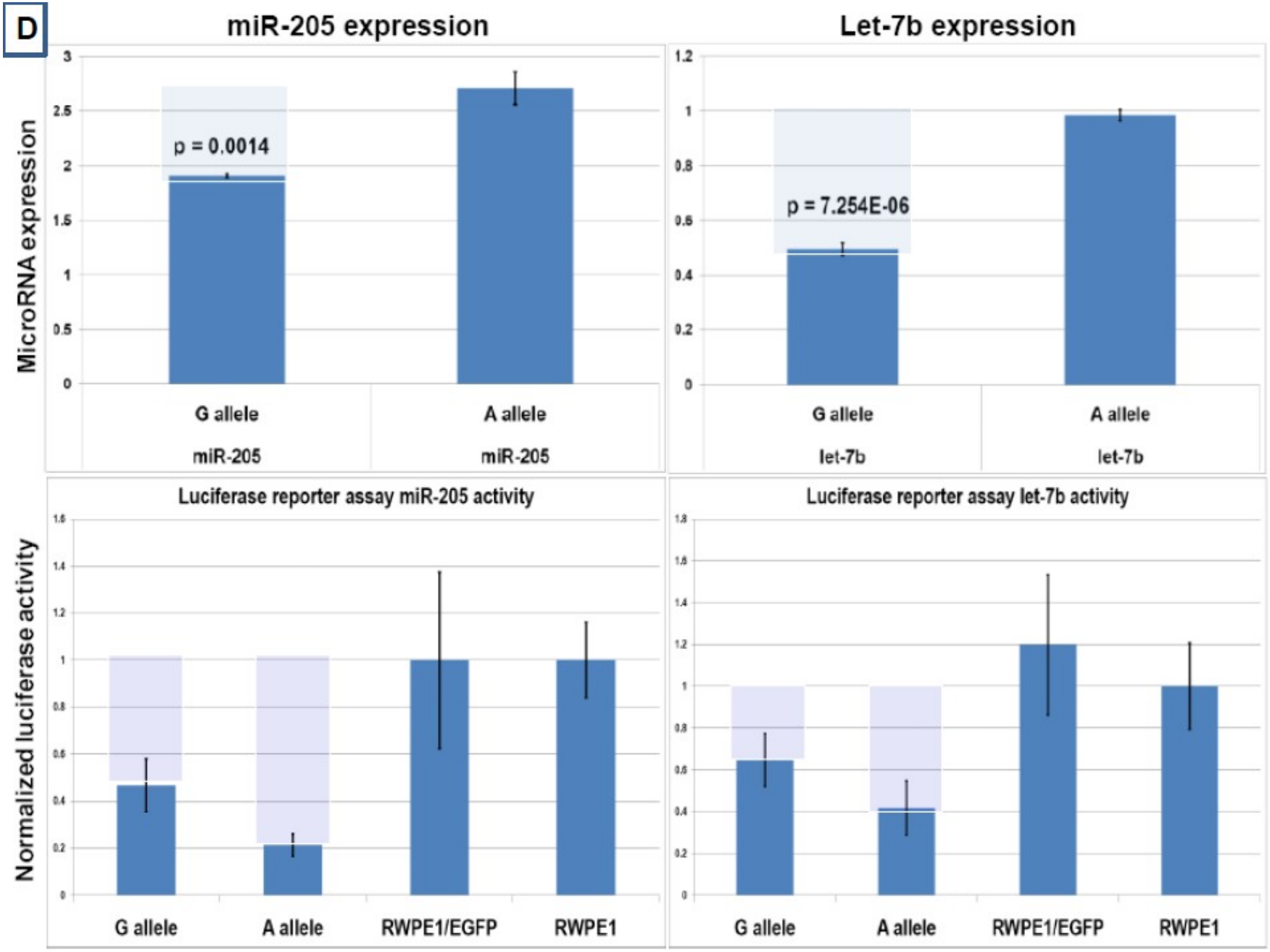

Figure 6.

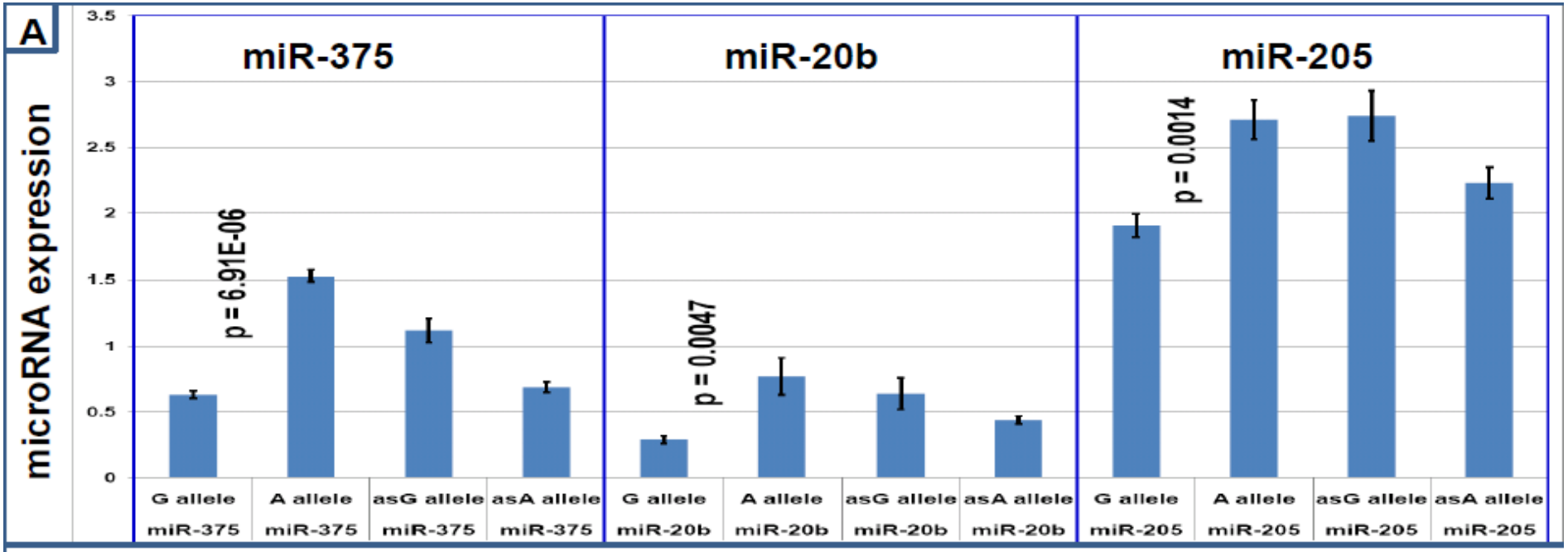

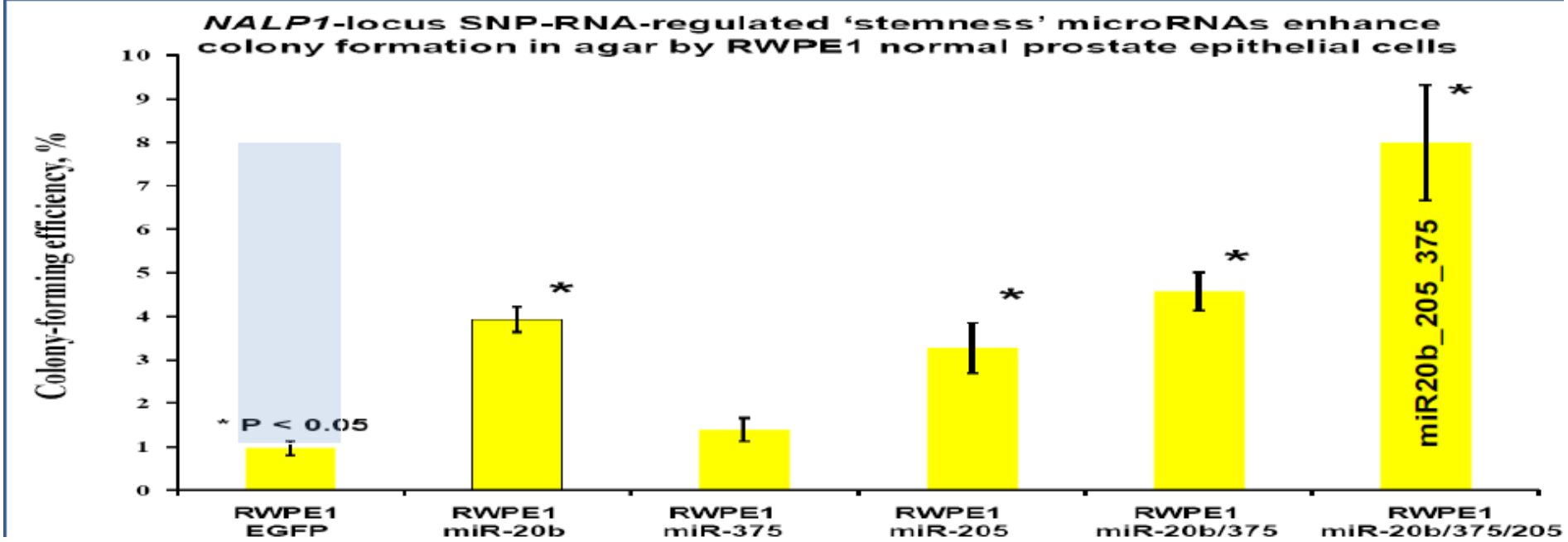

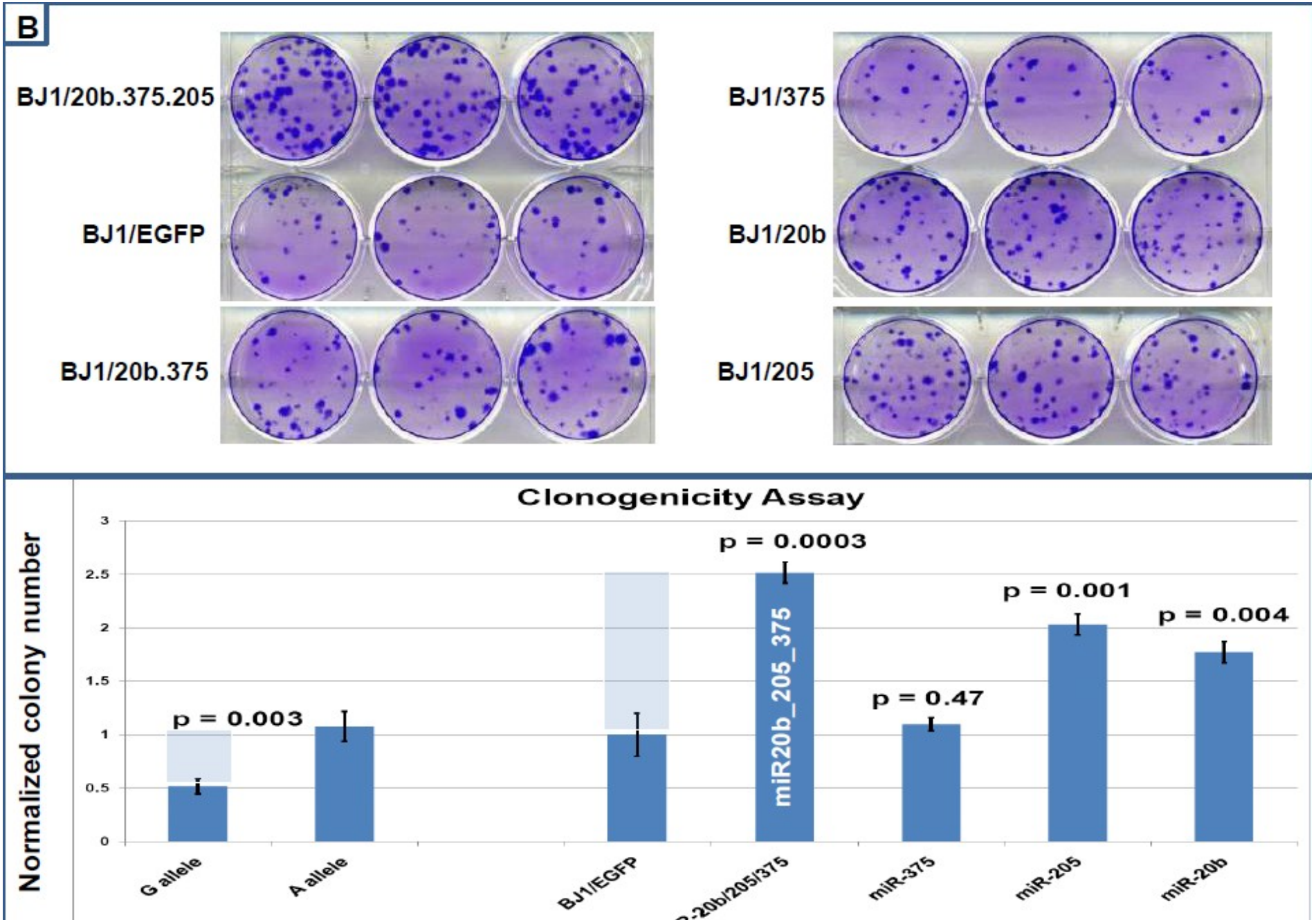

C

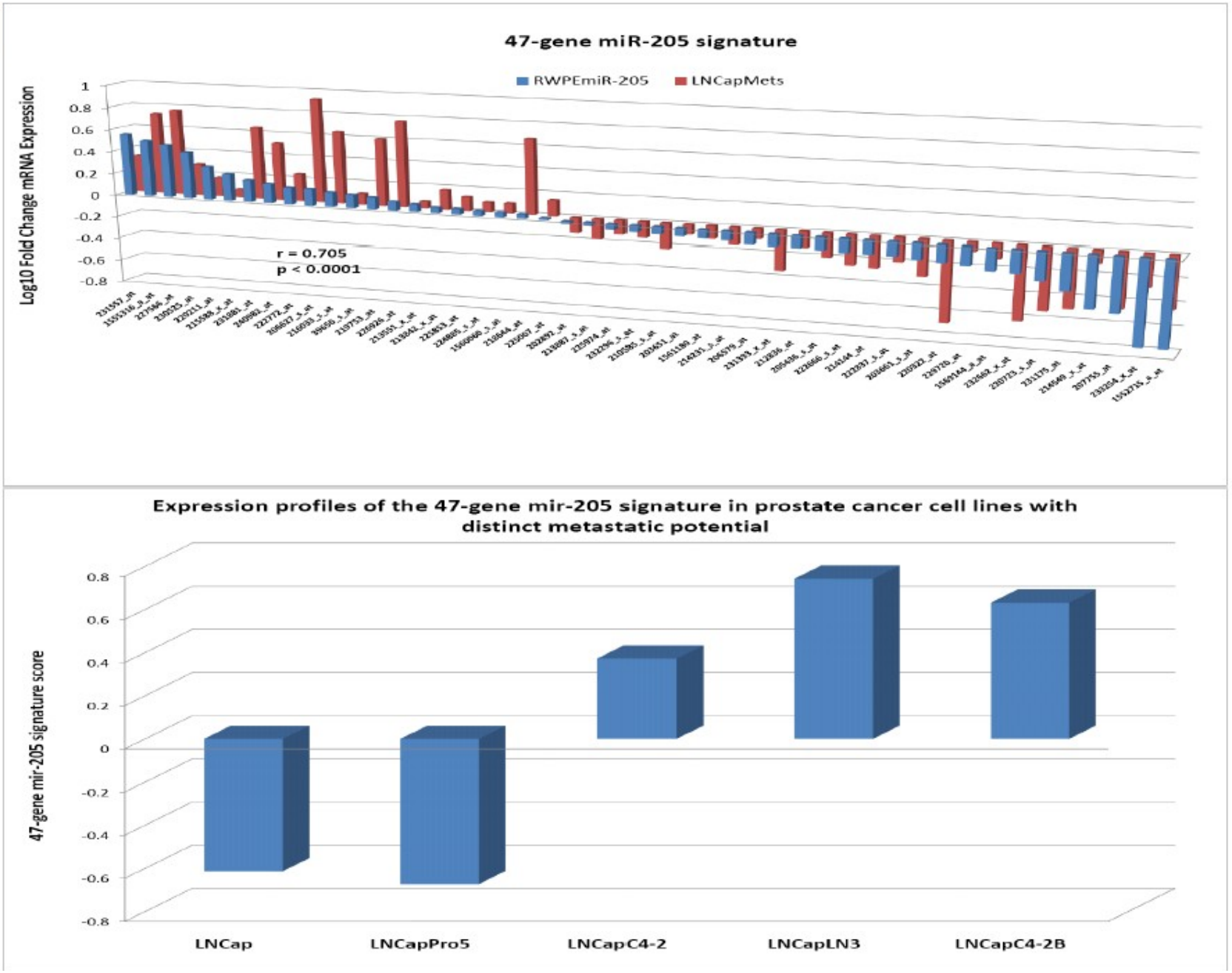

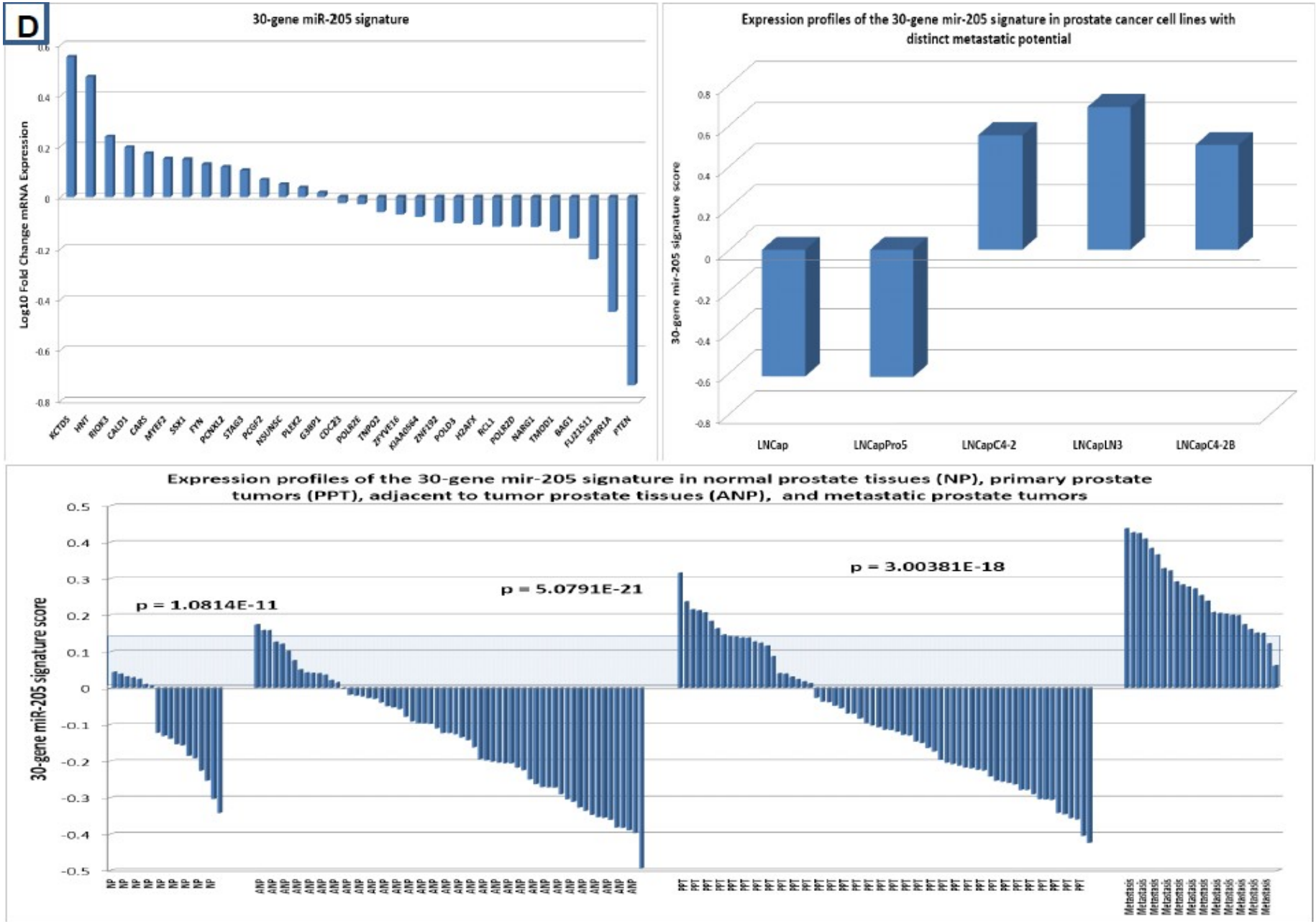

E

Relapse-free survival of 79 prostate cancer patients with distinct expression profiles of the 16-gene miR-205 signature